Molecular Cell

Article

Loop-extruding Smc5/6 organizes transcription-induced positive DNA supercoils

Graphical abstract

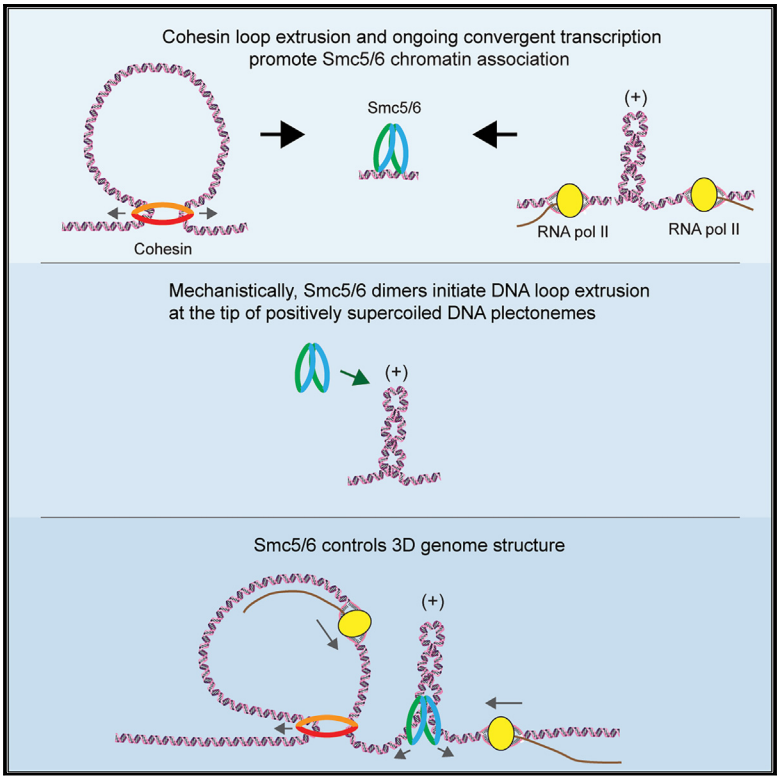

Highlights

- Transcription positions Smc5/6 at the base of cohesin-dependent chromosome loops
- Transcription-induced positive supercoiling triggers Smc5/6 chromosomal association
- Smc5/6 loads on the tip of positively supercoiled DNA plectonemes to extrude loops
- Smc5/6 controls the 3D organization of positively supercoiled chromosome regions

Authors

Kristian Jeppsson, Biswajit Pradhan, Takashi Sutani, ..., Katsuhiko Shirahige, Eugene Kim, Camilla Björkegren

Correspondence

jeppsson@iqb.u-tokyo.ac.jp (K.J.), eugene.kim@biophys.mpg.de (E.K.), camilla.bjorkegren@ki.se (C.B.)

In brief

The eukaryotic SMC complexes cohesin, condensin, and the Smc5/6 complex are DNA-loop-extruding motors. Jeppsson et al. show that Smc5/6 preferentially initiates loop extrusion on overtwisted, also called positively supercoiled, DNA. In cells, Smc5/6 is found at sites with transcription-induced positive supercoils, where it controls the spatial organization of chromosomes.

Jeppsson et al., 2024, Molecular Cell *84*, 867–882
March 7, 2024
https://doi.org/10.1016/j.molcel.2024.01.005

CellPress

Molecular Cell

CellPress
OPEN ACCESS

Article

Loop-extruding Smc5/6 organizes transcription-induced positive DNA supercoils

Kristian Jeppsson,[1,2,3,6,*] Biswajit Pradhan,[4] Takashi Sutani,[3] Toyonori Sakata,[1,2,3] Miki Umeda Igarashi,[1,2] Davide Giorgio Berta,[1,5] Takaharu Kanno,[1,2] Ryuichiro Nakato,[3] Katsuhiko Shirahige,[1,2,3] Eugene Kim,[4,*] and Camilla Björkegren[1,2,*]

[1]Karolinska Institutet, Department of Cell and Molecular Biology, Biomedicum, Tomtebodavägen 16, 171 77 Stockholm, Sweden
[2]Karolinska Institutet, Department of Biosciences and Nutrition, Neo, Hälsovägen 7c, 141 83 Huddinge, Sweden
[3]Institute for Quantitative Biosciences, The University of Tokyo, 1-1-1 Yayoi, Bunkyo-ku, Tokyo 113-0032, Japan
[4]Max Planck Institute of Biophysics, 60438 Frankfurt am Main, Germany
[5]Present address: AstraZeneca, Pepparedsleden 1, 431 83 Mölndal, Sweden
[6]Lead contact
*Correspondence: jeppsson@iqb.u-tokyo.ac.jp (K.J.), eugene.kim@biophys.mpg.de (E.K.), camilla.bjorkegren@ki.se (C.B.)
https://doi.org/10.1016/j.molcel.2024.01.005

SUMMARY

The structural maintenance of chromosomes (SMC) protein complexes—cohesin, condensin, and the Smc5/6 complex (Smc5/6)—are essential for chromosome function. At the molecular level, these complexes fold DNA by loop extrusion. Accordingly, cohesin creates chromosome loops in interphase, and condensin compacts mitotic chromosomes. However, the role of Smc5/6's recently discovered DNA loop extrusion activity is unknown. Here, we uncover that Smc5/6 associates with transcription-induced positively supercoiled DNA at cohesin-dependent loop boundaries on budding yeast (*Saccharomyces cerevisiae*) chromosomes. Mechanistically, single-molecule imaging reveals that dimers of Smc5/6 specifically recognize the tip of positively supercoiled DNA plectonemes and efficiently initiate loop extrusion to gather the supercoiled DNA into a large plectonemic loop. Finally, Hi-C analysis shows that Smc5/6 links chromosomal regions containing transcription-induced positive supercoiling in *cis*. Altogether, our findings indicate that Smc5/6 controls the three-dimensional organization of chromosomes by recognizing and initiating loop extrusion on positively supercoiled DNA.

INTRODUCTION

The Smc5/6 complex (Smc5/6) is part of the eukaryotic family of structural maintenance of chromosomes (SMCs) protein complexes, which also includes cohesin and condensin. These multi-subunit complexes hydrolyze ATP to create DNA loops by extrusion.[1–3] Cohesin performs so-called symmetrical extrusion, i.e., it reels in DNA from both sides of a growing loop, while condensin creates loops by one-sided extrusion.[1,2] Similar to cohesin, Smc5/6 performs two-sided loop extrusion. However, unlike cohesin and condensin, which extrude loops as monomers, Smc5/6 extrudes loops in the form of dimers of complexes and instead translocates along DNA in the monomeric form.[3] In line with loop extrusion taking place *in vivo*, cohesin promotes the formation of chromosome loops and topological associated domains (TADs) and condensin compacts mitotic chromosomes.[4–7] It remains, however, unknown whether Smc5/6 loop extrusion activity also regulates the three-dimensional structure of chromosomes.

Smc5/6 cellular function remains mostly unknown, but appears to be executed during late S- to G2/M-phase and prevents the formation of segregation-inhibiting chromatid linkages.[8–10] Smc5/6 is also needed for DNA damage repair and controls homologous recombination.[11–13] On *Saccharomyces cerevisiae* (*S. cerevisiae*) chromosomes, Smc5/6 co-localizes with cohesin in between convergently oriented gene pairs,[14,15] which in turn limits the size of cohesin loops by creating boundaries that block the progression of the extruding complex.[16,17] Interestingly, Smc5/6 chromosomal association depends on cohesin, whereas cohesin binding is not disrupted by inactivation of Smc5/6.[14] Both complexes also appear on chromosomes in early S-phase, show the most prominent binding in G2/M, and are removed at anaphase.[12,14,18] However, while cohesin is highly enriched between most convergently oriented gene pairs along chromosome arms, strong Smc5/6 association is only observed in centromere-proximal regions in wild-type cells,[12,14] indicating that cohesin influences Smc5/6 chromosomal association indirectly.

Smc5/6 function has also been connected to DNA supercoiling and sister chromatid intertwinings (SCIs). SCIs are formed if the replication machinery rotates with the turn of the DNA helix during replication, which causes the newly produced sister chromatids to wrap around each other (Figure S1A). DNA supercoiling arises when translocating polymerases or helicases unwind the DNA double helix, for example, during transcription

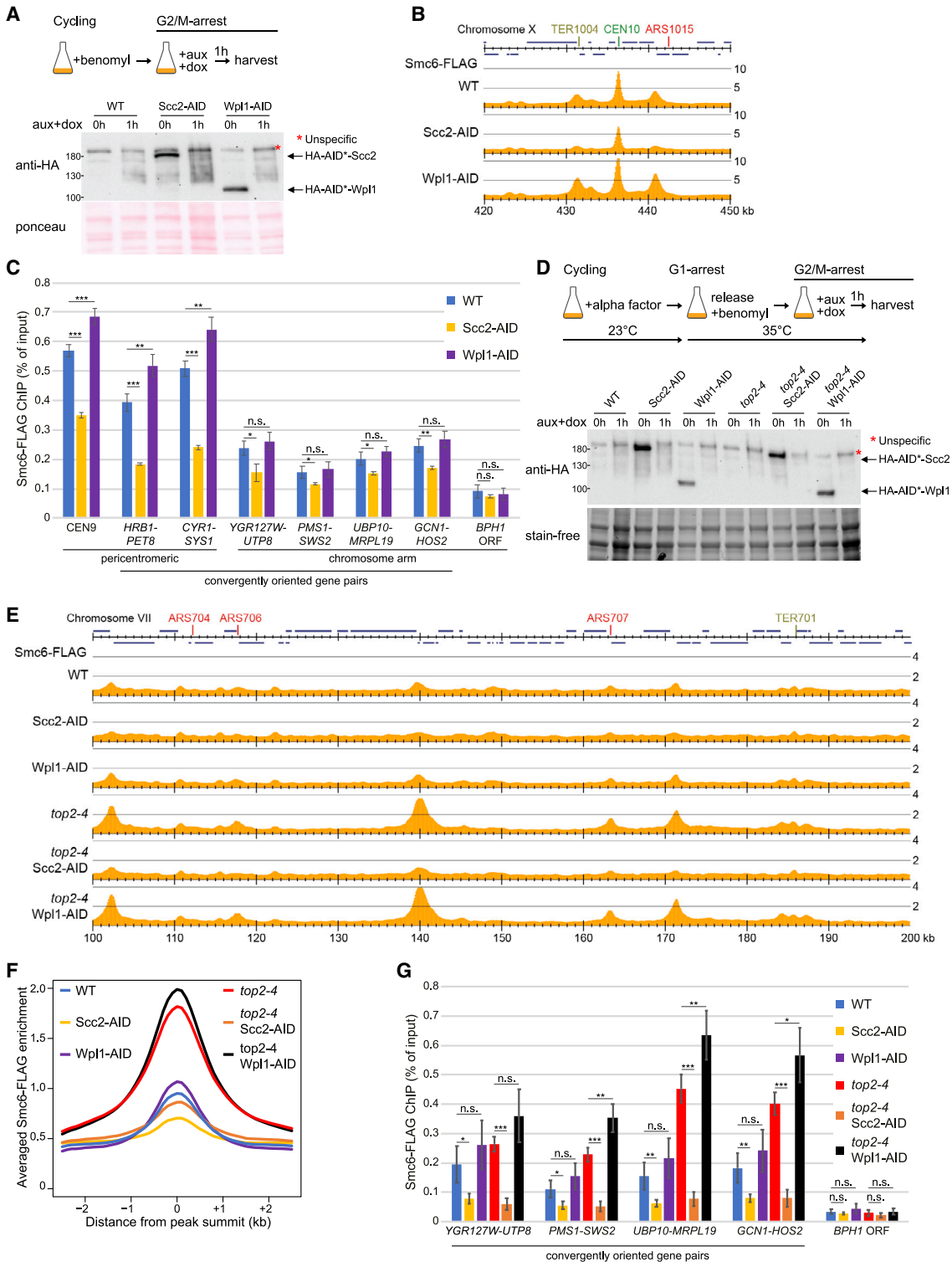

Figure 1. Smc5/6 chromosomal association depends on loop-extruding cohesin

(A) Experimental setup used in (B) and (C) and Figures S1D and S1F (up) and corresponding western blot showing Scc2 and Wpl1 depletion (down). The 0-h auxin + doxycycline western blot control samples were harvested immediately before the addition of the chemicals.

(B) Smc6-FLAG enrichment in the centromeric region of chromosome 10, 420–450 kb from left telomere, in wild-type, Scc2-, or Wpl1-depleted G2/M cells, as determined by ChIP-seq. The y axis shows fold enrichment of ChIP/input in linear scale, and the x axis shows chromosomal positions. Blue horizontal bars in the uppermost genomic region panel denote open reading frames (ORFs), CEN core centromere, ARS replication origins, and TER replication termination sites.

(legend continued on next page)

(reviewed in Wang).[19] This causes overtwisting of the DNA (i.e., positive supercoiling) ahead and undertwisting (i.e., negative supercoiling) behind the transcription machinery, which at high levels of twist can fold into a structure of writhe called a plectonemic supercoil (Figures S1B and S1C). DNA supercoils and SCIs are resolved by type I (e.g., Top1) and type II (e.g., Top2) topoisomerase enzymes that create transient single- and double-strand DNA breaks, respectively. Both Top2 and Top1 can perform supercoil relaxation, while SCIs can only be removed by Top2. Thus, inhibition of Top2 specifically during DNA replication leads to an accumulation of SCIs, while both Top2 and Top1 must be inhibited to block supercoil relaxation.[19] Interestingly, when Top2 is inhibited during replication, Smc5/6 binding is no longer restricted to centromere-proximal regions but appears in between convergently oriented genes all along *S. cerevisiae* chromosome arms, thereby showing a more comprehensive co-localization with cohesin.[14,20] In contrast, when Top2 is inhibited in G2/M-arrested cells, after replication, no change in Smc5/6 distribution is observed.[14] This suggests that the presence of SCIs directly or indirectly controls the chromosomal association of Smc5/6. In addition, magnetic tweezer analysis reveals that Smc5/6 stabilizes both positive and negative supercoils, and *in vitro* pull-down experiments indicate that Smc5/6 preferentially entraps positively supercoiled plasmids.[21,22] Even if the reason why the two experimental systems provide different results remains unclear, the investigations suggest that Smc5/6 function is influenced by supercoiling. Altogether, this indicates that Smc5/6 function is connected to cohesin, SCIs, and supercoiling, but so far, the interrelationship between these factors has remained undetermined.

Prompted by our recent finding that Smc5/6 is a DNA loop extruder *in vitro*,[3] we have explored whether Smc5/6 controls the spatial organization of chromosomes. This has revealed a specialized genome organization function, where Smc5/6 creates intrachromosomal links between chromosomal regions that contain transcription-induced positive supercoiling. These regions are found at the base of cohesin-dependent loops, and loop-extruding cohesin is also found to control Smc5/6 chromosomal binding. Single-molecule imaging confirms the preferential binding of Smc5/6 to positive supercoils and further reveal that dimers of Smc5/6 initiate DNA loop extrusion at the tip of positively supercoiled DNA plectonemes. Altogether, our work establishes that all eukaryotic SMC complexes control the spatial organization of chromosomes and reveals mechanistic insights into Smc5/6 cellular function and its connection to cohesin, SCIs, and DNA supercoiling.

RESULTS

Smc5/6 chromosomal association depends on loop-extruding cohesin

Given that Smc5/6 chromosomal localization depends on cohesin, and cohesin has been shown to create loops with boundaries at Smc5/6 binding sites, Smc5/6 might be controlled by loop-extruding cohesin.[14,16,23] To test this, we performed chromatin immunoprecipitation sequencing (ChIP-seq) and ChIP-qPCR analyses of Smc6 after depletion of Scc2 and Wpl1, the cohesin loader and unloader, respectively.[24–26] When Scc2 is depleted in G2/M-arrested cells, the majority of cohesin-mediated loops are lost,[17] while sister chromatid cohesion, the canonical function of cohesin,[18,27] remains unperturbed.[24] The analysis showed that Scc2 depletion in G2/M significantly reduces Smc5/6 enrichment around centromeres, indicating a dependency on cohesin loop extrusion (Figures 1A–1C and S1D–S1F). Supporting this, Wpl1 depletion, which causes cohesin to remain on chromosomes and form more and longer loops, significantly increased Smc5/6 enrichment around centromeres (Figures 1A–1C and S1D–S1F).[17,28]

Smc5/6 accumulates at cohesin sites along chromosome arms in response to the increase of SCIs caused by DNA replication in the absence of Top2 function.[14,20] To test whether this association is also under the control of loop-extruding cohesin, we used cells carrying a temperature-sensitive Top2 allele (*top2-4*). The cells were first arrested in G1 at permissive temperature and thereafter released through S-phase into G2/M-arrest at restrictive temperature (35°C) to inhibit Top2-4 protein activity, thereby triggering the accumulation of SCIs. Finally, Scc2 or Wpl1 was depleted in the G2/M-arrested *top2-4* cells, after which samples for ChIP-seq analysis were harvested (Figures 1D and S1G). Like the association around centromeres in wild-type cells, Scc2 depletion significantly reduced Smc5/6 chromosomal association in *top2-4* cells (Figures 1E–1G). Moreover, depletion of Wpl1 caused an accumulation of Smc5/6 to levels even higher than after Top2 inhibition alone (Figures 1E–1G). Together, this shows that the accumulation of Smc5/6 at cohesin sites in response to higher levels of SCIs also requires loop-extruding cohesin.

Smc5/6 chromosomal association requires ongoing transcription

The association of Smc5/6 to intergenic regions (IGRs) in between convergently oriented genes suggests that the complex might be regulated by transcription. We therefore investigated

(C) Smc6-FLAG enrichment at centromere 9 and in intergenic regions, between the indicated convergent gene pairs, and within the *BPH1* ORF, a Smc5/6-"non-binding site," as determined by ChIP-qPCR analysis of wild-type, Scc2-, or Wpl1-depleted G2/M cells. N = 3, n.s.: $p > 0.05$, * $p \leq 0.05$, ** $p \leq 0.01$, *** $p \leq 0.001$. The error bars denote standard deviation.

(D) Experimental setup used in (E)–(G) (up) and corresponding western blot showing Scc2 and Wpl1 depletion, as in (A) (down).

(E) Smc6-FLAG enrichment along the arm of chromosome 7, 100–200 kb from left telomere, in wild-type and *top2-4* mutated G2/M-arrested cells, with or without Scc2 or Wpl1 depletion. Annotations as in (B).

(F) Averaged Smc6-FLAG enrichment at Smc5/6 binding sites based on the analysis in (E).

(G) Smc6-FLAG enrichment in intergenic regions between indicated convergent gene pairs, as determined by ChIP-qPCR analysis of G2/M-arrested wild-type and *top2-4* mutated cells, with or without Scc2 or Wpl1 depletion. N = 3, n.s.: $p > 0.05$, * $p \leq 0.05$, ** $p \leq 0.01$, *** $p \leq 0.001$. The error bars denote standard deviation.

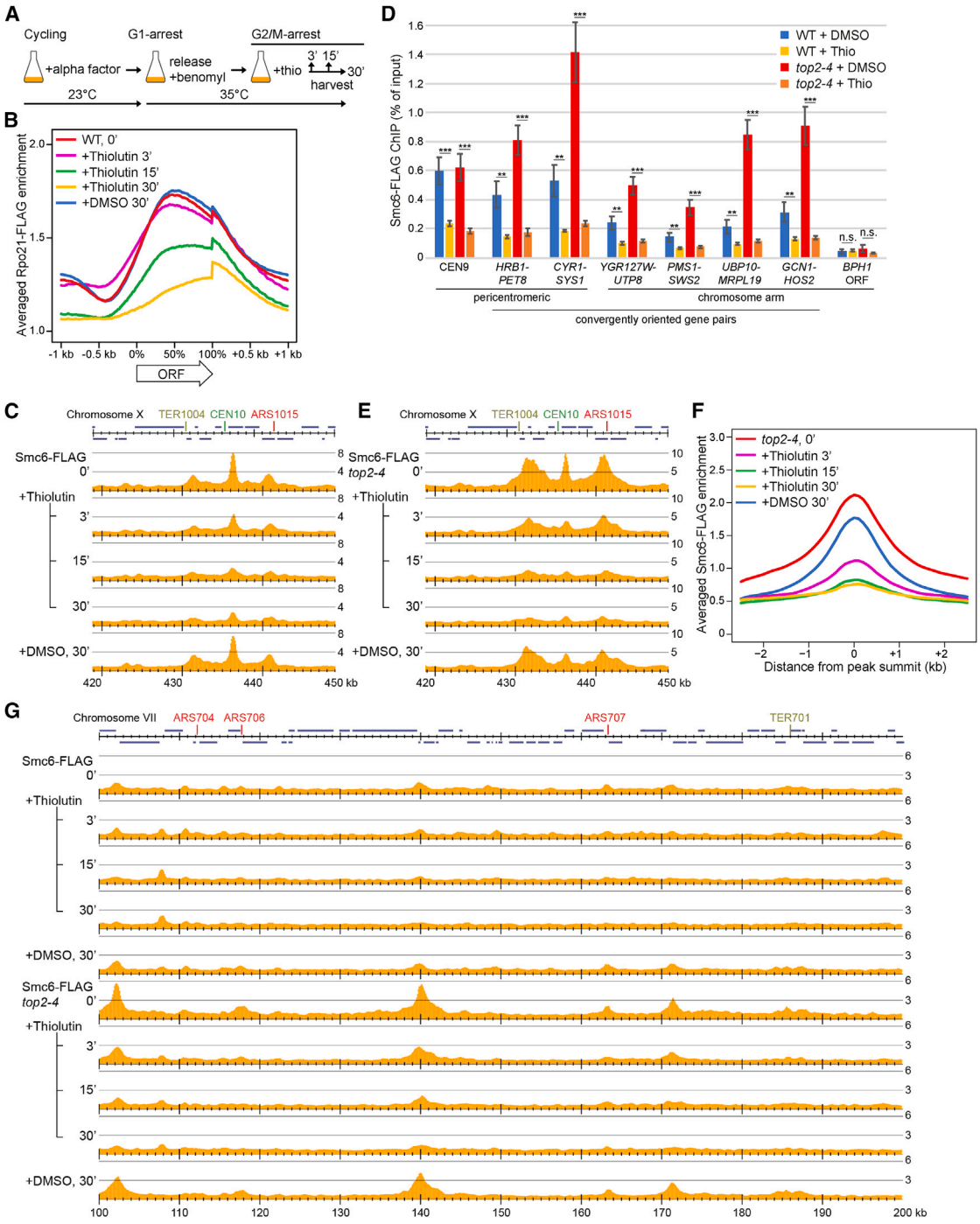

Figure 2. Smc5/6 chromosomal association requires ongoing transcription

(A) Experimental setup used for experiments displayed in (B)–(G) and Figures S1H, S1I, and S2A–S2I.

(B) Averaged Rpo21-FLAG enrichment within, and 1 kb up- and downstream of, ORFs, with or without preceding thiolutin treatment during indicated periods.

(C) Smc6-FLAG enrichment in the centromeric region of chromosome 10, 420–450 kb from left telomere, in wild-type cells, with or without indicated periods of thiolutin treatment. Annotations as in Figure 1B.

(D) Smc6-FLAG enrichment at centromere 9 and in intergenic regions, between the indicated convergent gene pairs, and within the *BPH1* ORF, a Smc5/6-non-binding site, as determined by ChIP-qPCR analysis of wild-type and *top2-4* cells, with or without preceding 30 min thiolutin treatment. N = 3, n.s.: $p > 0.05$, * $p \leq 0.05$, ** $p \leq 0.01$, *** $p \leq 0.001$. The error bars denote standard deviation.

(legend continued on next page)

the Smc5/6 chromosomal binding pattern after 3-, 15-, and 30-min treatment with the transcriptional inhibitor thiolutin (Figure 2A). Control experiments show that this causes RNA polymerase II (RNA Pol II) to dissociate from chromosomes (Figures 2B and S1H). Thiolutin treatment caused a rapid and significant reduction of Smc6 around centromeres in G2/M-arrested wild-type cells (Figures 2C, 2D, S2A, and S2B). Transcription inhibition also quickly and efficiently removed Smc5/6 from cohesin sites at centromeric regions and along chromosome arms in *top2-4* cells (Figures 2D–2G, S2A, S2C, and S2D). Moreover, even if initially low, Smc5/6 association in between convergently oriented genes along chromosome arms in wild-type cells was also rapidly reduced by thiolutin (Figures 2G, S2D, and S2E). In contrast, cohesin's chromosomal association was more modestly affected by transcription inhibition in G2/M-arrested wild-type or *top2-4* cells (Figures S1I and S2F–S2I), in line with previous findings.[17,23] We also investigated Smc5/6 localization by ChIP-qPCR after inhibition of the temperature-sensitive RNA Pol II allele *rpb1-1* in wild-type and Top2-auxin-induced degron (AID) cells, which confirmed that Smc5/6 dissociates from chromosomes following transcription inhibition (Figures S2J–S2L). Together, the results indicate that Smc5/6's chromosomal association requires ongoing transcription of convergently oriented genes in addition to cohesin loop extrusion. Given that the transcribing RNA polymerases overwind the DNA ahead of them, the mechanism that recruits Smc5/6 to IGRs in between convergently oriented genes could involve positively supercoiled DNA. This said, the transcription-dependent chromosomal positioning could also reflect that RNA Pol II creates a boundary for loop-extruding cohesin,[17,29] which in turn regulates Smc5/6 binding.

Positive supercoiling recruits Smc5/6 to chromosomes

To conclusively assess whether DNA supercoiling directly controls Smc5/6 chromosomal positioning independently of cohesin, we replaced the promoters of the *MCR1-DBR1* convergent gene pair with the strong constitutive promoters P_{ADH1} and P_{GPD}, respectively (Figures 3A and S3A). This increased the transcription rates of *MCR1* ≈ 22-fold and *DBR1* ≈ 63-fold (Figure 3B), which will trigger an accumulation of positive supercoils between the genes.[30] Aware of the role of Smc5/6 during S-phase, we ensured that the promoter replacement did not interfere with cell cycle progression or resistance to replication stress (Figures S3B and S3C). ChIP experiments showed that without promoter replacement, some cohesin—but little, if any, Smc5/6—can be detected in between *MCR1* and *DBR1* (Figures 3C, 3D, S3A, and S3D). In sharp contrast, high levels of convergent transcription caused a site-specific recruitment of Smc5/6 to the IGR, while cohesin enrichment was reduced (Figures 3C, 3D, S3D, and S3E). Moreover, the induced Smc5/6 association between the highly expressed convergent gene pair remained unchanged when cohesin function was inhibited using the temperature-sensitive *scc1-73* allele (Figure 3E). Together, this indicates that Smc5/6 accumulation at this highly positively supercoiled chromosomal region occurs independently of cohesin. To test this further, we replaced the P_{ADH1} promoter with $P_{Gal1-10}$ to enable inducible strong expression of *MCR1*, and thereby also cell cycle-specific induction of high convergent transcription (Figure 3F). Control experiments confirmed strong induction of *MCR1* upon galactose addition to the cell culture media (Figure S3F). Thereafter, cells were arrested in G1 or G2/M and convergent transcription was induced for 1 h, after which Smc5/6 localization was investigated by ChIP-qPCR. This revealed that inducible convergent transcription also triggers Smc5/6 recruitment between the gene pair, not only in G2/M but also in a G1-arrest, when cells contain very low levels of cohesin, and Smc5/6 is normally not detected between convergent gene pairs (Figures 3G and S3G–S3I). The association of Smc5/6 to an un-replicated chromosome in G1-arrested cells confirms that Smc5/6 recruitment caused by strong convergent transcription can occur independently of cohesin. Importantly, it also shows that Smc5/6 can bind chromosomes independently of any other G2/M-specific factor, such as the presence of SCIs.

To investigate the effect of positive DNA supercoiling on Smc5/6 association to unmodified genomic sites, the chromosomal association of the complex was analyzed after inactivation of either Top1, Top2, or the two topoisomerases in combination in G2/M-arrested cells (Figures 4A and S3J). By blocking the activity of Top1 and Top2 simultaneously, supercoil resolution is impaired to the extent that the transcription process is affected[19] and transcription-induced positive supercoils accumulate in between convergently oriented genes.[30] Following depletion of Top1, Smc5/6 binding remained unaltered (Figures 4B–4D). Inactivation of Top2 after DNA replication, which does not increase the level of SCIs, did not lead to Smc5/6 accumulation along chromosome arms (Figures 4B–4D), in line with previous findings.[14] However, Smc5/6 enrichment between convergently oriented genes was significantly increased after inactivation of both topoisomerases (Figures 4B–4D). In addition, the complex accumulated in broad peaks that spread into the flanking open reading frames (Figures 4B and 4C). This, together with the results obtained from the artificially highly expressed convergent gene pair, show that positive DNA supercoils determine Smc5/6 chromosomal positioning.

Transcription levels and length of surrounding genes govern Smc5/6 enrichment

To gain further insight into the regulation of Smc5/6's chromosomal distribution and enrichment level, we also performed multivariable analysis by computational machine learning using 47 defined chromosomal features (Table S4), which were organized into 8 groups according to their properties (Figure 5A). The analysis focused on all IGRs in the *S. cerevisiae* genome and was based on ChIP-seq of Smc5/6 and cohesin. When all combined, the defined features were sufficient to accurately

(E) Smc6-FLAG enrichment as in (C), but in *top2-4* cells.
(F) Averaged Smc6-FLAG enrichment at Smc5/6 binding sites based on the analysis in (G).
(G) Smc6-FLAG enrichment along the arm of chromosome 7, 100–200 kb from left telomere, in wild-type (up) and *top2-4* mutated (down) G2/M-arrested cells, with or without preceding thiolutin treatment during indicated periods. Annotations as in Figure 1B.

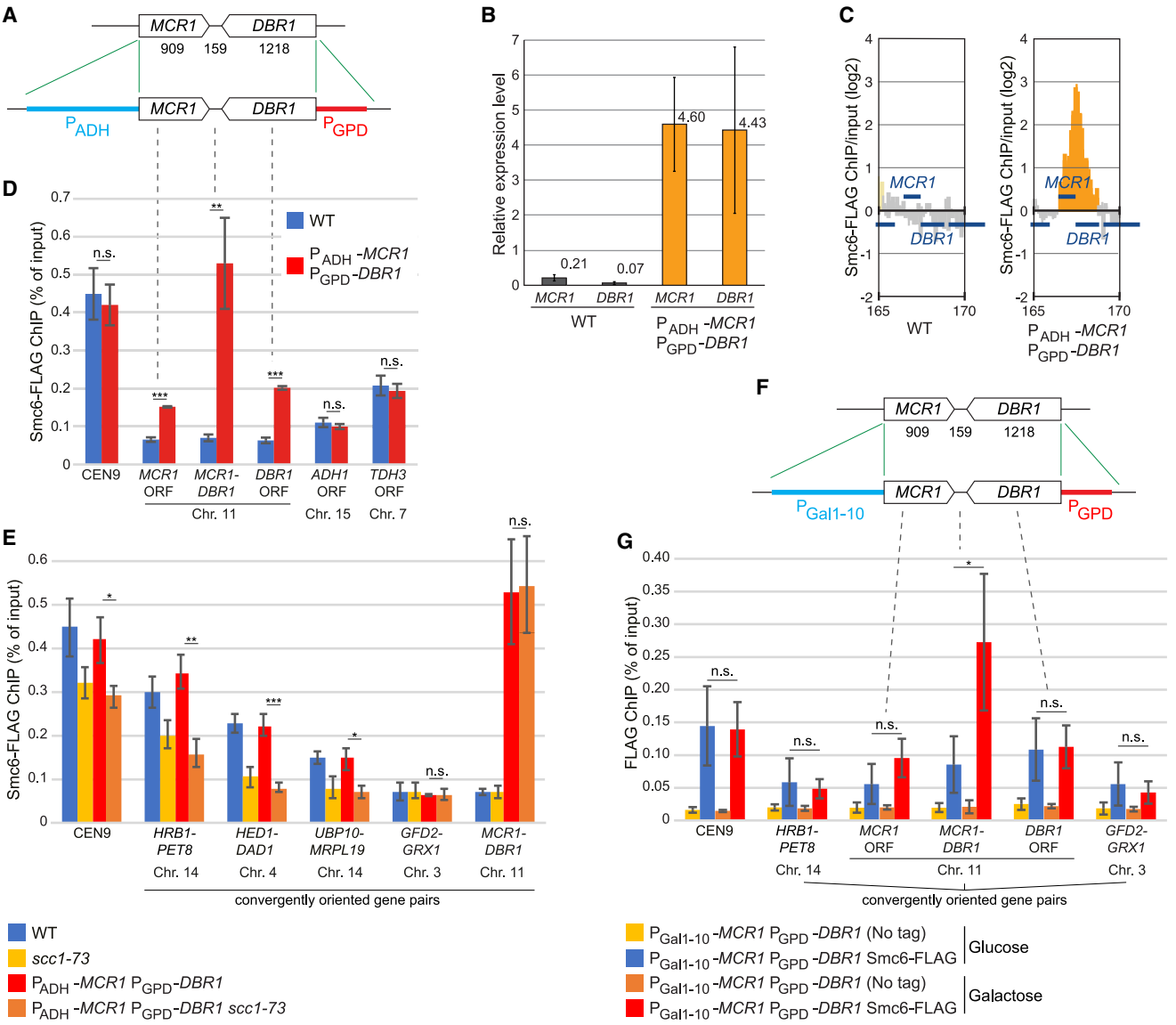

Figure 3. Positive supercoiling induced by site-specific high convergent transcription recruits Smc5/6 to chromosomes

(A) Genomic modifications used to create site-specific high convergent transcription. The size of *MCR1* and *DBR1* ORFs and the intervening intergenic region are indicated in number of base pairs.

(B) Relative expression levels of *MCR1* and *DBR1* as compared with *ACT1* before and after promoter replacement, determined by quantitative reverse-transcription PCR. N = 3, error bars indicate standard deviations.

(C) Smc6-FLAG enrichment between *MCR1* and *DBR1* before and after promoter replacement, determined by ChIP-on-chip. Blue vertical lines denote ORFs, the y axis shows fold enrichment of ChIP/input in $\log_2$ scale and the x axis chromosomal positions on chromosome 11.

(D) Smc6-FLAG enrichment at centromere 9 in the intergenic regions between the *MCR1-DBR1* convergent gene pair and within *MCR1*, *DBR1*, *ADH1*, *TDH3* ORFs, as indicated. The data were obtained by ChIP-qPCR analysis of cells with or without *MCR1* and *DBR1* promoter replacement. N = 3, n.s.: $p > 0.05$, ** $p \leq 0.01$, *** $p \leq 0.001$. The error bars denote standard deviation.

(E) As in (D) but in wild-type or *scc1-73* temperature-sensitive mutant background cells at centromere 9 and in between indicated convergent gene pairs, including the modified *MCR1-DBR1* site.

(F) Genomic modifications used to create site-specific, galactose-inducible high convergent transcription.

(G) Smc6-FLAG enrichment at centromere 9 at intergenic regions between indicated convergent gene pairs and within *MCR1* and *DBR1* ORFs, as indicated. The data were obtained by ChIP-qPCR analysis of G1-arrested cells with or without *MCR1* and *DBR1* promoter replacement, after 1 h in the presence of glucose or galactose. N = 3, n.s.: $p > 0.05$, * $p \leq 0.05$. The error bars denote standard deviation.

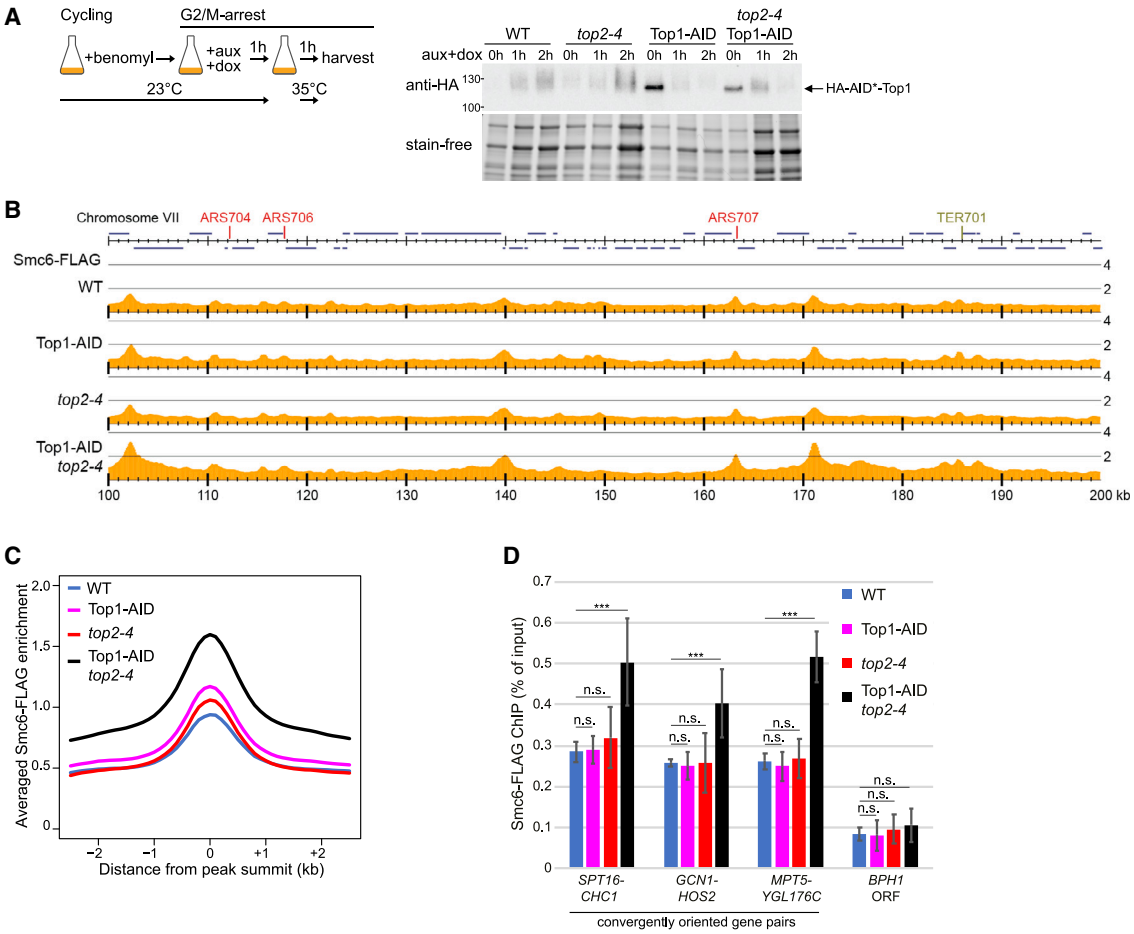

Figure 4. Positive supercoiling recruits Smc5/6 to endogenous chromosomal sites

(A) Experimental setup used in (B)–(D) and Figure S3J (left) and corresponding western blot showing Top1-depletion (right). The 0-h auxin + doxycycline western blot control samples were harvested immediately before the addition of the chemicals.

(B) Smc6-FLAG enrichment along the arm of chromosome 7, 100–200 kb from left telomere, in G2/M-arrested cells, with or without preceding Top1-depletion, *top2-4* inhibition, or both. Annotations as in Figure 1B.

(C) Averaged Smc6-FLAG enrichment at Smc5/6 binding sites, based on analysis in (B).

(D) Smc6-FLAG enrichment in intergenic regions between indicated convergent gene pairs and within the *BPH1* ORF, a Smc5/6-non-binding site, as determined by ChIP-qPCR analysis of the same cell types as in (B) and (C). N = 3, n.s.: $p > 0.05$, * $p \leq 0.05$, ** $p \leq 0.01$, *** $p \leq 0.001$. The error bars denote standard deviation.

predict the enrichment level of both Smc5/6 and cohesin at each IGR (Figure 5A). For cohesin, modeling solely based on group D features resulted in a good prediction (Figure 5A), which nicely reflects previous reports that cohesin enrichment mainly depends on the convergent orientation of surrounding genes.[15] The addition of group H features, which describe chromosome length and distance to centromeres and telomeres, had a significant positive impact on the predictive power of the analysis, likely reflecting the enrichment of cohesin in the centromeric area (Figures 5B and 5C; Table S4).[15] In line with the fact that Smc5/6 and cohesin show a high degree of co-localization on entangled chromosomes, the features describing convergent orientation of genes (feature group D) and positioning along chromosomes (feature group H) were also important to predict Smc5/6 chromosomal distribution in *top2-4* cells (Figures 5D and 5E). However, to accurately predict Smc5/6 enrichment in wild-type cells, the features describing transcription rates and length of the most proximal, adjoining convergent gene pair (feature group B) had to be included (Figures 5D and 5E). Investigation of each feature revealed that Smc5/6 enrichment was associated with higher expression and longer length of the adjacent genes (Table S4). Knowing that high transcription and longer genes induce more positive supercoiling,[31,32] this strengthens the notion that Smc5/6 is controlled directly by positive DNA supercoiling.

Smc5/6 initiates loop extrusion at the tip of positively supercoiled DNA plectonemes

To obtain a mechanistic understanding of Smc5/6's function and its association with positively supercoiled DNA, we performed single-molecule analysis that allows direct visualization of

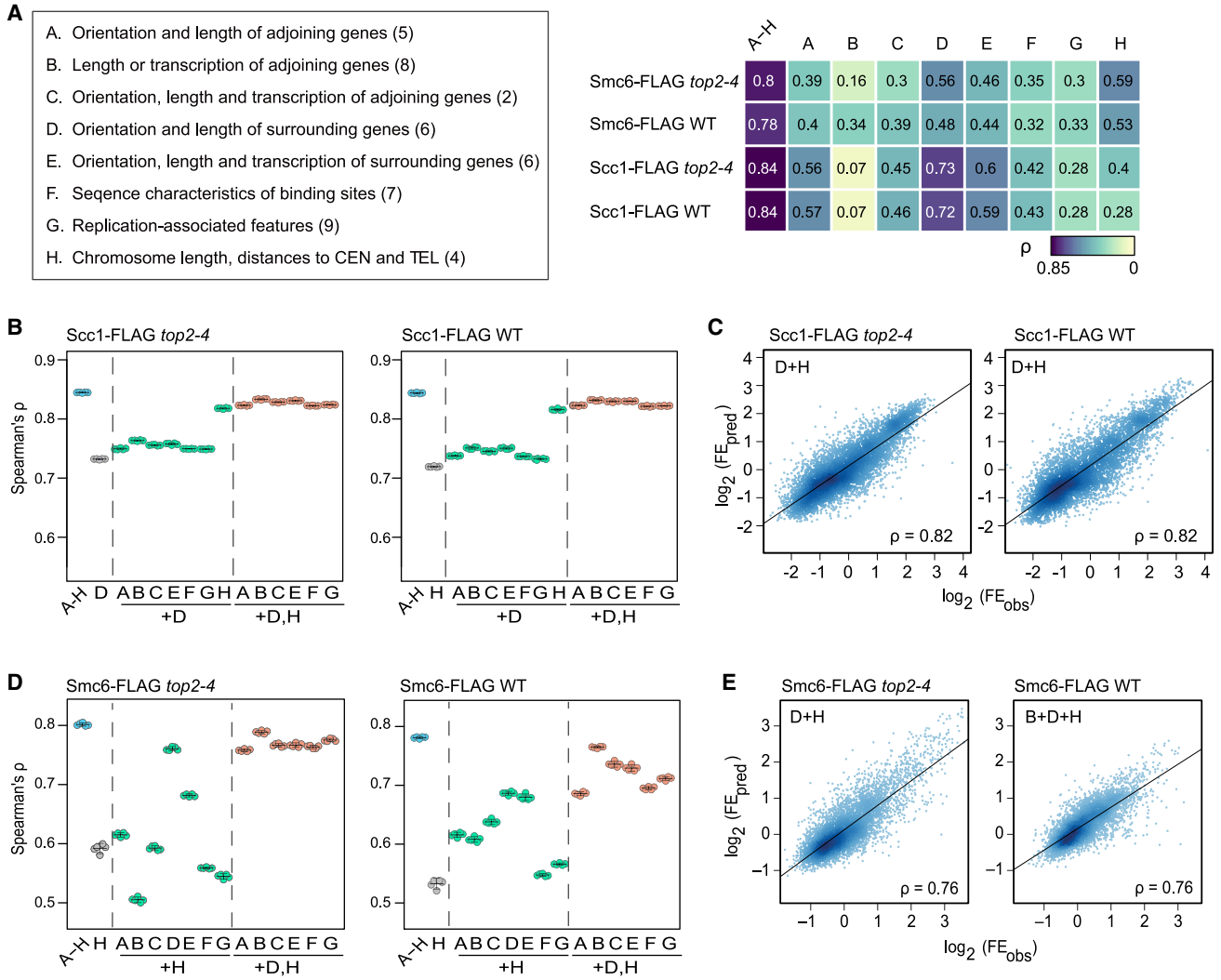

Figure 5. Transcription levels and gene length of surrounding genes govern Smc5/6 enrichment

(A) Left: groups of features used for modeling (see Table S4 for details). The number of features per group are indicated in parentheses. Right: the fold enrichment (FE) of Smc6 and Scc1 at each intergenic region in wild-type and *top2-4* mutated cells was modeled by machine learning. Groups of features used for model building are indicated at the top. Accuracy of the prediction was evaluated by Spearman's rank correlation coefficient (ρ) between predicted and observed FE values.

(B) Accuracy of prediction models for Scc1-FLAG enrichment in *top2-4* and wild-type cells using the indicated groups of features described in (A). 4-fold cross-validation was repeated 5 times with differently partitioned datasets, and the resulting correlation coefficients are plotted. The horizontal line indicates the mean, and whiskers show the 95% confidence interval.

(C) Representative prediction results of the analysis in (B). Observed and predicted FE values, FE_{obs} and FE_{pred}, respectively, were plotted in log_2 scale. Feature groups D and H were used to model Scc1-FLAG enrichment in both wild-type and *top2-4* cells.

(D) Analysis of Smc6-FLAG enrichment in *top2-4* and wild-type cells, as described in (B).

(E) Representative prediction results of analysis in (D), displayed as in (C). Feature groups D and H were used to model Smc6-FLAG enrichment in *top2-4* cells and groups B, D, and H for the modeling of Smc6-FLAG enrichment in wild-type cells.

Smc5/6 loop extrusion on supercoiled DNA attached to a passivated glass surface. Previously, we used this system to show that purified Smc5/6 can extrude DNA loops on nicked DNA as dimers of hexameric complexes (Smc5, Smc6, and Nse1-Nse4), while monomeric complexes translocate along DNA.[3] The Nse5 and Nse6 subcomplex (Nse5/6) promotes translocation (and reduces looping) of Smc5/6 by inhibiting dimerization of Smc5/6 hexamers. We therefore purified hexameric and octameric Smc5/6s, i.e., with and without Nse5/6, and determined their association and loop extrusion activity on positively and negatively supercoiled 42-kb DNA substrates stained by the intercalating SYTOX Orange (SxO) dye. Positive supercoiling was induced by adding SxO after restraining torsion release by tethering the DNA ends to the surface, and negative supercoils

CellPress
OPEN ACCESS

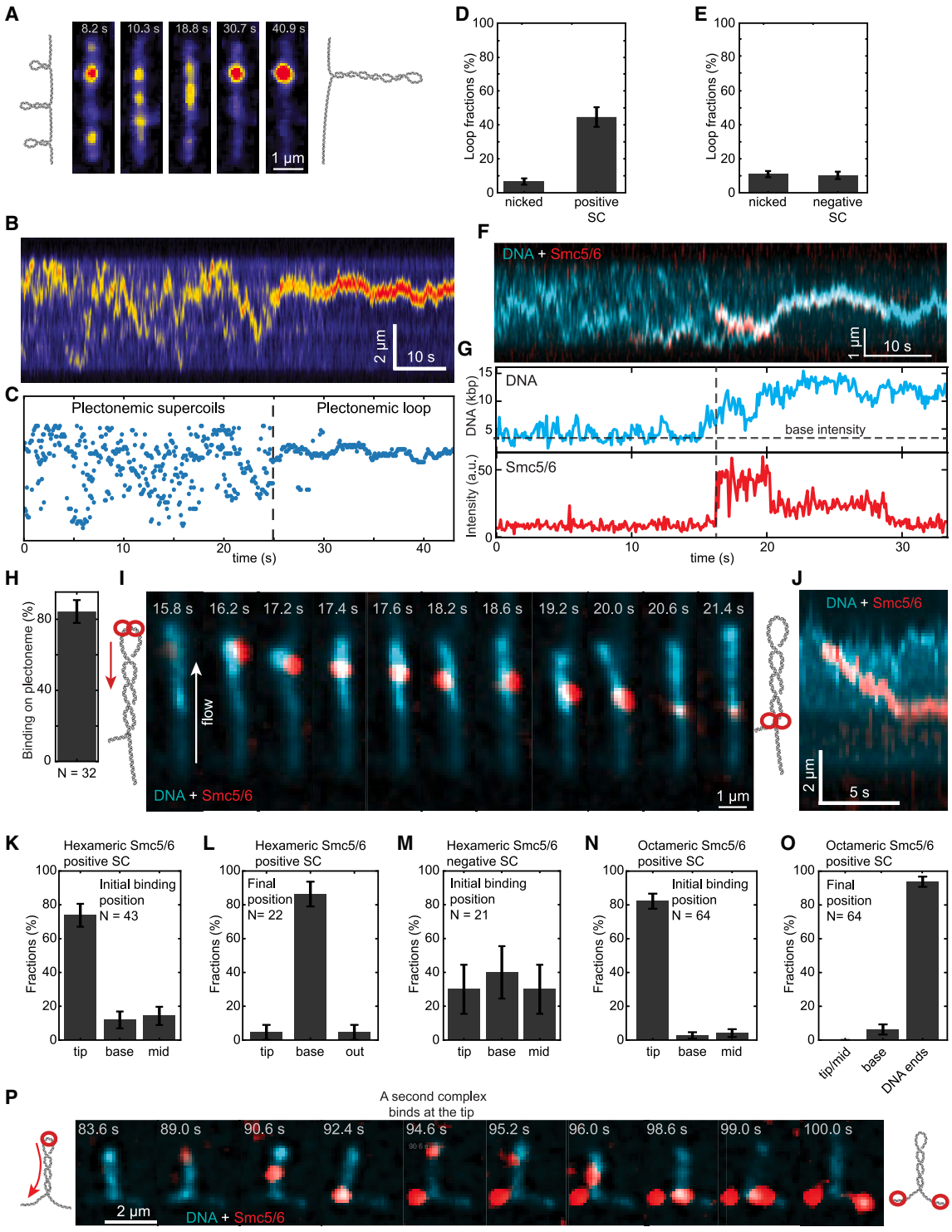

Figure 6. Smc5/6 preferentially binds and initiates DNA loop extrusion at the tip of positively supercoiled plectonemes

(A) Snapshots of positively supercoiled DNA stained with SYTOX Orange after the addition of 1 nM hexameric Smc5/6 in the presence of ATP.

(B and C) (B) A kymograph of the DNA and (C) puncta positions, corresponding to (A).

(D and E) The fraction of extruded loops by Smc5/6 per DNA molecule on positively (D) and negatively (E) supercoiled DNA, compared with nicked DNA.

(F) A kymograph of DNA (cyan) loop extrusion by labeled hexameric Smc5/6 (red) on positively supercoiled DNA, initially binding at a plectoneme and resulting in a single large plectonemic loop.

(G) Time trace of the DNA loop size and intensity of labeled Smc5/6 in (F).

(legend continued on next page)

were created by reducing dye concentration after attaching pre-stained DNA, as previously reported.[33] By using half of the SxO concentration that allowed maximum intercalation ($C_{1/2}$ = 300 nM) for generation and visualization of positive and negative supercoils, similar levels of dynamic plectonemes, observed as transient local maxima in DNA kymographs, were obtained (Figures S4A–S4C).

Upon the addition of hexameric Smc5/6 to positively supercoiled DNA, the dynamic plectonemes were rapidly gathered into a single stable loop by extrusion (Figures 6A–6C and S4D; Video S1). Strikingly, loop extrusion was 6.7 ± 2.0 times more likely to occur on positively supercoiled as compared with nicked DNA (Figure 6D). In contrast, loop extrusion initiation on negatively supercoiled DNA was not enhanced compared with that observed on nicked DNA (Figure 6E). The rate of loop extrusion on positively supercoiled DNA was modestly increased to 2.4 ± 1.3 kbp per s, as compared with 1.8 ± 1.1 kbp per s on nicked DNA (Figure S4E), although the difference was not statistically significant. This reveals that positive, but not negative, DNA supercoiling greatly enhances the Smc5/6 loop extrusion initiation rate.

Interestingly, analysis of fluorescently labeled hexameric Smc5/6 revealed that Smc5/6 initially binds to the dynamic, positively supercoiled plectonemes and, following the swift depletion of the smaller dynamic plectonemes, Smc5/6 overlaps with a single intensifying spot (Figures 6F–6H; Video S2). Bleaching dynamics of the labeled Smc5/6 after initiation of loop extrusion revealed a larger fraction (58% ± 8%) of two-step bleaching events as compared with single-step events (34% ± 7%), which, taken together with the labeling efficiency of 72%, confirms that Smc5/6 performs loop extrusion on positively supercoiled DNA as dimers of hexameric complexes, similar to the extrusion detected on nicked DNA (Figures 6F, 6G, and S4F–S4H and Pradhan et al.).[3]

Analysis using fluorescently labeled octameric Smc5/6, which primarily exhibits translocation in monomeric form and very low levels of DNA loop extrusion,[3] revealed that the binding of this version of Smc5/6 on supercoiled DNA was approximately 4 times higher as compared with nicked DNA (Figures S4I and S4J). As expected for translocating complexes, following initial binding, octameric Smc5/6 moved to the ends of the tethered DNA molecule (Figures S4I and S4K). Hence, the results show that preferential binding on positively supercoiled DNA is shared between the monomeric and dimeric forms of Smc5/6 and indicates that the enhanced looping probability on positively supercoiled DNA is due to increased binding of Smc5/6 dimers to positively supercoiled plectonemes.

Applying side-way buffer flow to the chamber pins the dynamic positive plectonemes into one single plectoneme,[34] thus allowing observation of binding and the subsequent loop extrusion dynamics of the labeled Smc5/6s along plectonemes. This revealed that hexameric Smc5/6 dimers initially associate to the tip of the positively supercoiled plectoneme and subsequently move downwards until they are found at the base of the loop (Figures 6I–6L; Video S3). The stalling at the base of the loop indicates that the downward movement reflects loop extrusion. In contrast with the preferred association to the tip of positively supercoiled plectonemes, initial Smc5/6 binding on flow-stretched, negatively supercoiled plectonemes occurred at random positions (Figure 6M). Moreover, analyzing octameric Smc5/6, which primarily exhibits translocation along DNA,[3] revealed a similar preference to initially bind the tip of positively supercoiled plectonemes (Figures 6N and 6P). However, these complexes continue moving downward along the plectoneme and bypass the base to reach the ends of the tethered DNA molecule (Figures 6O and 6P; Video S4), demonstrating the typical behavior of translocation.

Altogether, the results remarkably show that both monomers and dimers of Smc5/6 specifically recognize the tip of positively supercoiled DNA plectonemes. Thereafter, monomers translocate away from the plectoneme, while Smc5/6 dimers efficiently initiate loop extrusion to gather the surrounding supercoiled DNA into one large plectonemic loop.

Smc5/6 links positively supercoiled chromosomal loci

The fact that Smc5/6 preferentially initiates loop extrusion on the tip of positively supercoiled DNA *in vitro* (Figure 6), opens for that Smc5/6 performs loop extrusion at transcription-induced positively supercoiled chromosomal loci *in vivo* (Figures 1, 2, 3, and 4). To explore this hypothesis, Hi-C analysis was performed in G2/M-arrested cells that were depleted for Smc5 and Smc6 from the preceding G1-phase (Figures 7A and S5A–S5C). Supporting the idea that Smc5/6 performs DNA loop extrusion *in vivo*, the Hi-C analysis revealed a small but significant and reproducible reduction of chromosomal *cis* interactions in the Smc5/6-depleted cells (Figures 7B–7D and S5D). The Smc5/6-mediated *cis* interactions were found genome-wide within a distance span of 10–80 kb (Figures 7D and S5D). In contrast, Smc5/6 does not contribute to cohesin-mediated loops because these remained intact after the depletion (Figure 7E). Together, this shows that Smc5/6 has a clear but mild influence on chromosomal organization in wild-type cells, in line with the relatively low detection of the complex along chromosome arms.

Our results suggest that the accumulation of Smc5/6 on transcription-induced, positively supercoiled DNA can be further strengthened by the presence of SCIs (Figure 2). If Smc5/6 performs loop extrusion at these sites, SCIs are expected to increase the level of chromosome *cis* interactions. To test this idea, Hi-C analysis was performed on G2/M-arrested cells,

(H) The fraction of labeled hexameric Smc5/6 binding to plectonemes, with the remaining fraction binding outside the plectonemes.
(I and J) Binding of labeled hexameric Smc5/6 (red) to a positively supercoiled plectoneme and following DNA (cyan) loop extrusion under buffer side-flow (I), and the corresponding kymograph (J).
(K and L) Initial (K) and final (L) binding positions of labeled hexameric Smc5/6 on positively supercoiled DNA plectonemes under side-flow.
(M) Initial binding positions of labeled hexameric Smc5/6 on negatively supercoiled DNA.
(N and O) Initial (N) and final (O) binding positions of labeled octameric Smc5/6 on positively supercoiled DNA plectonemes under side-flow.
(P) Binding of labeled octameric Smc5/6 (red) to a positively supercoiled plectoneme (cyan) and following translocation under buffer side-flow.

CellPress
OPEN ACCESS

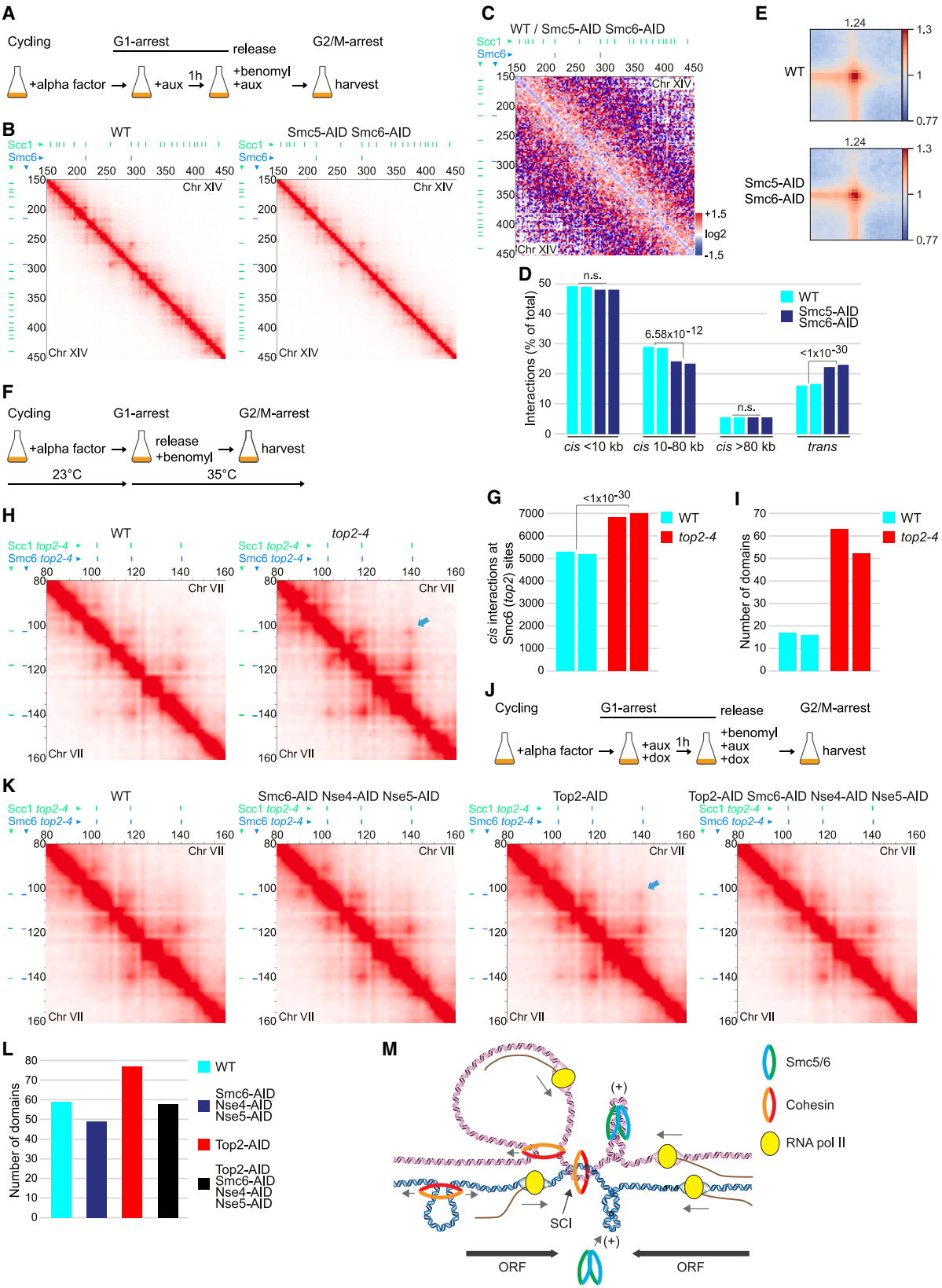

(legend on next page)

which had replicated in the absence of functional Top2 during the preceding S-phase (Figures 7F and S5E). The results revealed a significant increase in *cis* interactions at Smc5/6 binding sites that appear along chromosome arms after Top2 inhibition (Figure 7G). The increased *cis* interactions in *top2-4* cells occasionally linked neighboring Smc5/6 binding sites, indicative of a loop forming between them (Figures 7H and S5F–S5H). However, overall, the averaged strength of loops was not increased in *top2-4* cells (Figure S6A). Instead, the number of domains was strongly increased following Top2 inactivation (Figure 7I). These findings are in line with the idea that Smc5/6 performs loop extrusion after recruitment to positive supercoils on the entangled chromosomes, although rarely forming stable loops between neighboring detected binding sites. In further support of this finding, simultaneous depletion of Smc5/6 (Smc6-AID, Nse4-AID, Nse5-AID) and Top2 (Figures 7J and S6B–S6D), abolished the increase in *cis* interactions at Smc5/6 binding sites (Figures 7K, S6E, and S6F) and reduced the number of domains back to wild-type levels (Figure 7L). Together, this supports a model where Smc5/6 recognizes the tip of transcription-induced positively supercoiled DNA plectonemes that arise at cohesin loop boundaries and initiates DNA loop extrusion (Figure 7M).

DISCUSSION

Here, we show that Smc5/6 is recruited to transcription-induced positive DNA supercoils that appear at the base of cohesin-dependent chromosome loops in the genome and links positively supercoiled chromosomal loci in *cis*. Single-molecule imaging analysis provides detailed mechanistic insight into how Smc5/6 performs this function by revealing that dimers of Smc5/6 preferentially bind and initiate DNA loop extrusion at the tip of positively supercoiled plectonemes. This discovery of a chromosome organization function for Smc5/6 unites this so-far enigmatic complex with cohesin and condensin, which also control the spatial organization of chromosomes using DNA loop extrusion.

The starting point of our investigation was the earlier observations that Smc5/6 co-localizes with cohesin between convergently oriented genes and is connected to DNA supercoiling.[14,20–22] This suggested that the complex could be jointly controlled by cohesin and transcription-induced supercoiling and, accordingly, we found that Smc5/6 association is controlled by Scc2, Wpl1, and ongoing transcription (Figures 1 and 2). To tease out the role of transcription-induced DNA supercoiling in Smc5/6 chromosomal association, we genetically engineered a convergent gene pair in which both genes are transcribed at exceptionally high levels, thereby creating strong, positive supercoiling in the IGR (Figure 3). The finding that Smc5/6 is site-specifically recruited in between the two highly expressed, convergently oriented genes independently of cohesin (Figure 3), and the increase of Smc5/6 at endogenous binding sites after concomitant depletion of Top2 and Top1 (Figure 4), pinpoints positive supercoiling as the main underlying factor controlling the chromosomal binding pattern of the complex. Furthermore, single-molecule analysis establishes that Smc5/6 recognizes and preferentially binds the tip of positively supercoiled plectonemes to efficiently initiate loop extrusion, finally confirming positively supercoiled DNA plectonemes as preferred substrates for Smc5/6 (Figure 6).

Our observations that supercoils accumulate at the base of cohesin loops in the yeast genome gain support from investigations in mammalian cells showing that Top2 is active at TAD boundaries and that this activity is controlled by cohesin, the TAD boundary protein CTCF, and transcription.[35–37] Human Smc5/6 chromosomal association also follows that of cohesin, appearing on chromosomes before replication and remaining until mitosis, when both complexes concentrate in the centromeric area.[10,38] Furthermore, Smc5/6 chromosomal enrichment

Figure 7. Smc5/6 links positively supercoiled chromosomal loci

(A) Experimental setup used in (B)–(E) and Figures S5A, S5B, and S5D.

(B) Normalized Hi-C contact maps (2 kb binning) showing *cis* interactions along the arm of chromosome 14, 150–450 kb from left telomere, in G2/M-arrested wild-type and Smc5/6-depleted (Smc5-AID, Smc6-AID) cells. Lines on top and to the left of the panels: green, cohesin binding sites; blue, Smc5/6 binding sites.

(C) Normalized Hi-C ratio maps (2 kb binning) comparing chromosome *cis* interactions in G2/M-arrested wild-type and Smc5/6-depleted cells along the same chromosomal regions as depicted in (B).

(D) Quantification of *cis* (<10, 10–80, >80 kb) and *trans* interactions in G2/M-arrested wild-type and Smc5/6-depleted cells.

(E) Pile-up plots of averaged *cis* interactions in wild-type and Smc5/6-depleted cells between all pairs of cohesin sites situated 20–40 kb apart on chromosome arms.

(F) Experimental setup used in (G)–(I), Figures S5E, S5F, and S6A.

(G) Quantification of *cis* interactions (>10 kb) in wild-type and *top2-4* cells, anchored at Smc5/6 chromosome arm binding sites in *top2-4* cells.

(H) Normalized Hi-C contact maps (2 kb binning) showing *cis* interactions along the arm of chromosome 7, 80–160 kb from left telomere, in G2/M-arrested wild-type and *top2-4* cells. Lines on top and to the left of the panels: green, cohesin binding sites in *top2-4* mutant; blue, Smc5/6 binding sites in *top2-4* mutant; light blue arrow: example of increased *cis* interactions between Smc5/6 binding sites in *top2-4* cells.

(I) Number of domains in G2/M-arrested wild-type and *top2-4* cells.

(J) Schematic description of the experimental setup used in (K)–(L) and Figures S6B, S6C, S6E, and S6F.

(K) Normalized Hi-C contact maps (2 kb binning) showing *cis* interactions along the arm of chromosome 7, 80–160 kb from left telomere, in wild-type, Smc6-AID Nse4-AID Nse5-AID triple depletion, Top2-AID, and Top2-AID Smc6-AID Nse4-AID Nse5-AID quadruple depletion cells. Lines on top and to the left of the panels: green, cohesin binding sites in *top2-4* mutant; blue, Smc5/6 binding sites in *top2-4* mutant; light blue arrow: example of increased Smc5/6-dependent *cis* interactions between Smc5/6 binding sites in Top2-AID cells.

(L) Number of domains in G2/M-arrested wild-type, Smc6-AID Nse4-AID Nse5-AID triple depletion, Top2-AID, and Top2-AID Smc6-AID Nse4-AID Nse5-AID quadruple depletion cells.

(M) A model summarizing that cohesin loop extrusion, transcription, gene orientation, and chromosome entanglements (SCIs) contribute to the formation of positively supercoiled DNA plectonemes, which are recognized by dimers of hexameric Smc5/6 that initiates loop extrusion.

was also recently shown to be reduced upon transcription inhibition,[39] well in line with a highly conserved regulation of the complex in human and yeast cells.

Comparison of Smc5/6 binding patterns with that of the bacterial protein GapR, which binds positive supercoiling in the form of overtwisted DNA,[40] also reveals interesting similarities. When expressed in yeast, GapR is found at the 3′ end of most genes, is enriched in between convergently oriented genes, and positively correlates with transcription strength.[31] Consequently, GapR is also found at most cohesin binding sites, including those in the pericentromeric region. These observations support the notion that Smc5/6 is found in regions where chromosomal DNA is positively supercoiled. In addition, the GapR binding pattern indicates that positive supercoiling can be generated from upstream co-oriented genes and, similarly, Smc5/6 positioning and enrichment are not only influenced by the most proximal gene pair but also by the orientation of genes up to 10 kb away from the binding sites (feature group D, Figure 5; Table S4). This said, the preferential association of Smc5/6 to certain cohesin sites, in comparison with the more wide-spread distribution of GapR, suggests that Smc5/6 associates with a specific feature of positive supercoiling. Based on our observation that Smc5/6 preferentially recognizes the tip of positively supercoiled plectonemes (Figure 6), Smc5/6 potentially indicates the positions where these fundamental, but so-far elusive, chromosomal structures are formed or stabilized.

Because plectoneme formation requires a certain threshold of overtwisting, Smc5/6 is expected to be enriched in regions of high levels of positive supercoiling. Accordingly, exceptionally strong convergent transcription triggers the association of Smc5/6, which can also occur in G1-arrested cells and in the absence of cohesin (Figure 3). In addition, Smc5/6 should be detected at sites where other features facilitate the transition of overtwisting into plectonemes. One such feature would be factors that confine the superhelical twist, i.e., prevent it from spreading over larger chromosomal regions, which reduces the local level of twist. Interestingly, analysis of the effects of supercoiling on transcription in budding yeast suggests that supercoils are more confined on longer chromosomes and far away from chromosome ends, which mimics Smc5/6 distribution in wild-type cells.[14,20,41] Similarly, Smc5/6 accumulation at the base on cohesin loops and along intertwined chromatids suggests that cohesin confines transcription-induced supercoiling at the base of the loops and that this confinement is strengthened by SCIs.

Another question emanating from our investigation is how Smc5/6 specifically recognizes the tip of positively supercoiled plectonemes. Interestingly, we find that the mechanism for this recognition resides within the monomeric form of the complex because not only loop extrusion by Smc5/6 dimers but also translocation by monomers preferentially start at the tip of positively supercoiled plectonemes (Figure 6). Full disclosure of this process will demand detailed structural analysis, but it is interesting to notice that condensin also preferentially binds and loop extrudes positively supercoiled DNA.[34] However, while Smc5/6 performs two-sided loop extrusion in the form of a dimer of complexes, condensin loop extrusion is one-sided and is executed by monomeric complexes. The rate of condensin loop extrusion was also lowered by supercoiling, which was not observed for Smc5/6. Thus, even if the initial recognition of the positively supercoiled DNA might be similar, the following reaction will differ. Our Hi-C analysis suggests that, after loading, Smc5/6 uses loop extrusion to reel in DNA (Figure 7), which occasionally can bring two Smc5/6 binding sites together in the three-dimensional space. This said, the finding that chromosome intertwining leads to an Smc5/6-dependent increase in domains, but does not affect loops, suggests that the extrusion process is most often disrupted before reaching all the way to the neighboring Smc5/6 binding sites. The fact that Smc5/6 promotes segregation of entangled chromosomes[14] might indicate that this extrusion activity supports chromosome segregation and viability, an interesting focus for future studies.

Another interesting outcome of the initial Smc5/6 loading at the tip of positive plectonemes can be proposed, based on a recent study suggesting that Smc5/6 relies on positive supercoiling when acting as a viral restriction factor.[39] This function leads to transcriptional silencing on small circular episomal DNA, which has been suggested to depend on topological entrapment of DNA by Smc5/6.[42–44] Based on this, our finding that Smc5/6 specifically recognizes the tip of positively supercoiled plectonemes (Figure 6) might disclose the mechanism by which the complex initiates topological entrapment and viral restriction. After the initial binding at the plectoneme, Smc5/6 could either entrap the DNA molecule immediately or initiate loop extrusion or translocation, to later be converted into the topological entrapment binding mode.

Taken together, this investigation uncovers Smc5/6's function *in vivo* and explains the role of the complex's recently discovered loop extrusion activity. Crucially, the analysis also shows that transcription-induced positive supercoiling is not only a problem for topoisomerases to resolve but also acts as a central regulator of three-dimensional chromosome organization via Smc5/6.

Limitations of the study

Even if the presented results support the notion that Smc5/6 acts on positively supercoiled chromosomal regions folded into plectonemic structures, the study is limited by the lack of an alternative assay to detect such structures *in vivo*. In addition, given that ongoing transcription is required for Smc5/6 chromosomal positioning, it is difficult to exclude the possibility that the presence of the RNA Pol II machinery and nascent RNA molecules contribute to the detected Smc5/6 enrichment by a mechanism that is separate from the generation of positive supercoiling. In principle, the chromosomal positioning of Smc5/6 could be controlled by the secondary effect of positive supercoiling, and/or enhanced by the presence of the transcription machinery or nascent RNA molecules, even if the single-molecule analysis revealing that Smc5/6 directly recognizes the tip of positively supercoiled plectonemes argues against these alternatives.

STAR★METHODS

Detailed methods are provided in the online version of this paper and include the following:

- KEY RESOURCES TABLE

SUPPLEMENTAL INFORMATION

Supplemental information can be found online at https://doi.org/10.1016/j.molcel.2024.01.005.

ACKNOWLEDGMENTS

We thank C. Dekker and J. van der Torre for sharing the plasmids and the protocol for making the 42-kb coilable DNA construct. The study was funded by JSPS Postdoctoral Fellowship for Overseas Researchers, FY2016 (to K.J.); Max Planck Society and European Research Council starting grant number 101076914 (to E.K.); JST CREST grant number JPMJCR18S5 and JSPS KAKENHI grant numbers 20H05686 and 20H05940 (to K.S.); JSPS KAKENHI grant number 21K06012 (to T. Sutani); and Swedish Cancer Foundation, Swedish Research Council, and Centre for Innovative Medicine (CIMED) (to C.B.).

AUTHOR CONTRIBUTIONS

K.J. and C.B. conceived the initial ideas and developed the study together with all co-authors. K.J. performed all ChIP, RNA sequencing (RNA-seq), and Hi-C experiments, except for the ChIP-qPCR experiments presented in Figures 4D, 3E, 3G, S3E, and S3H, which were executed by M.U.I. and D.G.B., respectively. T.K. purified and labeled Smc5/6 for single-molecule analyses. B.P. performed the single-molecule experiments and data analysis, T. Sutani executed the machine learning analysis, and T. Sakata, R.N., K.J., and K.S. performed and developed the bioinformatic analysis of ChIP and Hi-C analyses. E.K. supervised the single-molecule imaging part of the project. K.J. and C.B. wrote the manuscript with input from all authors. K.J., K.S., E.K., and C.B. acquired funding.

DECLARATION OF INTERESTS

The authors declare no competing interests.

Received: July 17, 2023
Revised: November 16, 2023
Accepted: January 8, 2024
Published: January 30, 2024

REFERENCES

1. Davidson, I.F., Bauer, B., Goetz, D., Tang, W., Wutz, G., and Peters, J.M. (2019). DNA loop extrusion by human cohesin. Science *366*, 1338–1345.
2. Ganji, M., Shaltiel, I.A., Bisht, S., Kim, E., Kalichava, A., Haering, C.H., and Dekker, C. (2018). Real-time imaging of DNA loop extrusion by condensin. Science *360*, 102–105.
3. Pradhan, B., Kanno, T., Umeda Igarashi, M., Loke, M.S., Baaske, M.D., Wong, J.S.K., Jeppsson, K., Björkegren, C., and Kim, E. (2023). The Smc5/6 complex is a DNA loop-extruding motor. Nature *616*, 843–848.
4. Gibcus, J.H., Samejima, K., Goloborodko, A., Samejima, I., Naumova, N., Nuebler, J., Kanemaki, M.T., Xie, L., Paulson, J.R., Earnshaw, W.C., et al. (2018). A pathway for mitotic chromosome formation. Science *359*, eaao6135.
5. Rao, S.S.P., Huang, S.C., Hilaire, G.St.B., Engreitz, J.M., Perez, E.M., Kieffer-Kwon, K.R., Sanborn, A.L., Johnstone, S.E., Bascom, G.D., et al. (2017). Cohesin Loss Eliminates All Loop Domains. Cell *171*, 305–320.e24.
6. Schwarzer, W., Abdennur, N., Goloborodko, A., Pekowska, A., Fudenberg, G., Loe-Mie, Y., Fonseca, N.A., Huber, W., Haering, C.H., Mirny, L., et al. (2017). Two independent modes of chromatin organization revealed by cohesin removal. Nature *551*, 51–56.
7. Wutz, G., Várnai, C., Nagasaka, K., Cisneros, D.A., Stocsits, R.R., Tang, W., Schoenfelder, S., Jessberger, G., Muhar, M., Hossain, M.J., et al. (2017). Topologically associating domains and chromatin loops depend on cohesin and are regulated by CTCF, WAPL, and PDS5 proteins. EMBO J. *36*, 3573–3599.
8. Menolfi, D., Delamarre, A., Lengronne, A., Pasero, P., and Branzei, D. (2015). Essential Roles of the Smc5/6 Complex in Replication through Natural Pausing Sites and Endogenous DNA Damage Tolerance. Mol. Cell *60*, 835–846.
9. Torres-Rosell, J., De Piccoli, G., Cordon-Preciado, V., Farmer, S., Jarmuz, A., Machin, F., Pasero, P., Lisby, M., Haber, J.E., and Aragón, L. (2007). Anaphase onset before complete DNA replication with intact checkpoint responses. Science *315*, 1411–1415.
10. Venegas, A.B., Natsume, T., Kanemaki, M., and Hickson, I.D. (2020). Inducible Degradation of the Human SMC5/6 Complex Reveals an Essential Role Only during Interphase. Cell Rep. *31*, 107533.
11. Irmisch, A., Ampatzidou, E., Mizuno, K., O'Connell, M.J., and Murray, J.M. (2009). Smc5/6 maintains stalled replication forks in a recombination-competent conformation. EMBO J. *28*, 144–155.
12. Betts Lindroos, H.B., Ström, L., Itoh, T., Katou, Y., Shirahige, K., and Sjögren, C. (2006). Chromosomal association of the Smc5/6 complex reveals that it functions in differently regulated pathways. Mol. Cell *22*, 755–767.
13. Torres-Rosell, J., Machín, F., Farmer, S., Jarmuz, A., Eydmann, T., Dalgaard, J.Z., and Aragón, L. (2005). SMC5 and SMC6 genes are required for the segregation of repetitive chromosome regions. Nat. Cell Biol. *7*, 412–419.
14. Jeppsson, K., Carlborg, K.K., Nakato, R., Berta, D.G., Lilienthal, I., Kanno, T., Lindqvist, A., Brink, M.C., Dantuma, N.P., Katou, Y., et al. (2014). The chromosomal association of the smc5/6 complex depends on cohesion and predicts the level of sister chromatid entanglement. PLoS Genet. *10*, e1004680.
15. Lengronne, A., Katou, Y., Mori, S., Yokobayashi, S., Kelly, G.P., Itoh, T., Watanabe, Y., Shirahige, K., and Uhlmann, F. (2004). Cohesin relocation from sites of chromosomal loading to places of convergent transcription. Nature *430*, 573–578.
16. Costantino, L., Hsieh, T.S., Lamothe, R., Darzacq, X., and Koshland, D. (2020). Cohesin residency determines chromatin loop patterns. eLife *9*, e59889.

17. Jeppsson, K., Sakata, T., Nakato, R., Milanova, S., Shirahige, K., and Björkegren, C. (2022). Cohesin-dependent chromosome loop extrusion is limited by transcription and stalled replication forks. Sci. Adv. *8*, eabn7063.

18. Michaelis, C., Ciosk, R., and Nasmyth, K. (1997). Cohesins: chromosomal proteins that prevent premature separation of sister chromatids. Cell *91*, 35–45.

19. Wang, J.C. (2002). Cellular roles of DNA topoisomerases: a molecular perspective. Nat. Rev. Mol. Cell Biol. *3*, 430–440.

20. Kegel, A., Betts-Lindroos, H., Kanno, T., Jeppsson, K., Ström, L., Katou, Y., Itoh, T., Shirahige, K., and Sjögren, C. (2011). Chromosome length influences replication-induced topological stress. Nature *471*, 392–396.

21. Gutierrez-Escribano, P., Hormeño, S., Madariaga-Marcos, J., Solé-Soler, R., O'Reilly, F.J., Morris, K., Aicart-Ramos, C., Aramayo, R., Montoya, A., Kramer, H., et al. (2020). Purified Smc5/6 Complex Exhibits DNA Substrate Recognition and Compaction. Mol. Cell *80*, 1039–1054.e6.

22. Serrano, D., Cordero, G., Kawamura, R., Sverzhinsky, A., Sarker, M., Roy, S., Malo, C., Pascal, J.M., Marko, J.F., and D'Amours, D. (2020). The Smc5/6 Core Complex Is a Structure-Specific DNA Binding and Compacting Machine. Mol. Cell *80*, 1025–1038.e5.

23. Garcia-Luis, J., Lazar-Stefanita, L., Gutierrez-Escribano, P., Thierry, A., Cournac, A., García, A., González, S., Sánchez, M., Jarmuz, A., Montoya, A., et al. (2019). FACT mediates cohesin function on chromatin. Nat. Struct. Mol. Biol. *26*, 970–979.

24. Ciosk, R., Shirayama, M., Shevchenko, A., Tanaka, T., Toth, A., Shevchenko, A., and Nasmyth, K. (2000). Cohesin's binding to chromosomes depends on a separate complex consisting of Scc2 and Scc4 proteins. Mol. Cell *5*, 243–254.

25. Kueng, S., Hegemann, B., Peters, B.H., Lipp, J.J., Schleiffer, A., Mechtler, K., and Peters, J.M. (2006). Wapl controls the dynamic association of cohesin with chromatin. Cell *127*, 955–967.

26. Tedeschi, A., Wutz, G., Huet, S., Jaritz, M., Wuensche, A., Schirghuber, E., Davidson, I.F., Tang, W., Cisneros, D.A., Bhaskara, V., et al. (2013). Wapl is an essential regulator of chromatin structure and chromosome segregation. Nature *501*, 564–568.

27. Guacci, V., Koshland, D., and Strunnikov, A. (1997). A direct link between sister chromatid cohesion and chromosome condensation revealed through the analysis of MCD1 in S. cerevisiae. Cell *91*, 47–57.

28. Lopez-Serra, L., Lengronne, A., Borges, V., Kelly, G., and Uhlmann, F. (2013). Budding yeast Wapl controls sister chromatid cohesion maintenance and chromosome condensation. Curr. Biol. *23*, 64–69.

29. Banigan, E.J., Tang, W., van den Berg, A.A., Stocsits, R.R., Wutz, G., Brandão, H.B., Busslinger, G.A., Peters, J.M., and Mirny, L.A. (2023). Transcription shapes 3D chromatin organization by interacting with loop extrusion. Proc. Natl. Acad. Sci. USA *120*, e2210480120.

30. García-Rubio, M.L., and Aguilera, A. (2012). Topological constraints impair RNA polymerase II transcription and causes instability of plasmid-borne convergent genes. Nucleic Acids Res. *40*, 1050–1064.

31. Guo, M.S., Kawamura, R., Littlehale, M.L., Marko, J.F., and Laub, M.T. (2021). High-resolution, genome-wide mapping of positive supercoiling in chromosomes. eLife *10*, e67236.

32. Joshi, R.S., Piña, B., and Roca, J. (2012). Topoisomerase II is required for the production of long Pol II gene transcripts in yeast. Nucleic Acids Res. *40*, 7907–7915.

33. Kim, S.H., Ganji, M., Kim, E., van der Torre, J., Abbondanzieri, E., and Dekker, C. (2018). DNA sequence encodes the position of DNA supercoils. eLife *7*, e36557.

34. Kim, E., Gonzalez, A.M., Pradhan, B., van der Torre, J., and Dekker, C. (2022). Condensin-driven loop extrusion on supercoiled DNA. Nat. Struct. Mol. Biol. *29*, 719–727.

35. Canela, A., Maman, Y., Jung, S., Wong, N., Callen, E., Day, A., Kieffer-Kwon, K.R., Pekowska, A., Zhang, H., Rao, S.S.P., et al. (2017). Genome Organization Drives Chromosome Fragility. Cell *170*, 507–521.e18.

36. Gittens, W.H., Johnson, D.J., Allison, R.M., Cooper, T.J., Thomas, H., and Neale, M.J. (2019). A nucleotide resolution map of Top2-linked DNA breaks in the yeast and human genome. Nat. Commun. *10*, 4846.

37. Uusküla-Reimand, L., Hou, H., Samavarchi-Tehrani, P., Rudan, M.V., Liang, M., Medina-Rivera, A., Mohammed, H., Schmidt, D., Schwalie, P., Young, E.J., et al. (2016). Topoisomerase II beta interacts with cohesin and CTCF at topological domain borders. Genome Biol. *17*, 182.

38. Wendt, K.S., Yoshida, K., Itoh, T., Bando, M., Koch, B., Schirghuber, E., Tsutsumi, S., Nagae, G., Ishihara, K., Mishiro, T., et al. (2008). Cohesin mediates transcriptional insulation by CCCTC-binding factor. Nature *451*, 796–801.

39. Aurélie, D., Panis, G., Castrogiovanni, C., Prados, J., Baechler, B., and Strubin, M. (2023). Human Smc5/6 recognises transcription-generated positive DNA supercoils. Preprint at bioRxiv.

40. Guo, M.S., Haakonsen, D.L., Zeng, W., Schumacher, M.A., and Laub, M.T. (2018). A Bacterial Chromosome Structuring Protein Binds Overtwisted DNA to Stimulate Type II Topoisomerases and Enable DNA Replication. Cell *175*, 583–597.e23.

41. Joshi, R.S., Piña, B., and Roca, J. (2010). Positional dependence of transcriptional inhibition by DNA torsional stress in yeast chromosomes. EMBO J. *29*, 740–748.

42. Abdul, F., Diman, A., Baechler, B., Ramakrishnan, D., Kornyeyev, D., Beran, R.K., Fletcher, S.P., and Strubin, M. (2022). Smc5/6 silences episomal transcription by a three-step function. Nat. Struct. Mol. Biol. *29*, 922–931.

43. Kanno, T., Berta, D.G., and Sjögren, C. (2015). The Smc5/6 Complex Is an ATP-Dependent Intermolecular DNA Linker. Cell Rep. *12*, 1471–1482.

44. Taschner, M., Basquin, J., Steigenberger, B., Schäfer, I.B., Soh, Y.M., Basquin, C., Lorentzen, E., Räschle, M., Scheltema, R.A., and Gruber, S. (2021). Nse5/6 inhibits the Smc5/6 ATPase and modulates DNA substrate binding. EMBO J. *40*, e107807.

45. Langmead, B., and Salzberg, S.L. (2012). Fast gapped-read alignment with Bowtie 2. Nat. Methods *9*, 357–359.

46. Liaw, A., and Wiener, M. (2002). Classification and Regression by randomForest. R News *2/3*, 18–22.

47. Durand, N.C., Shamim, M.S., Machol, I., Rao, S.S., Huntley, M.H., Lander, E.S., and Aiden, E.L. (2016). Juicer Provides a One-Click System for Analyzing Loop-Resolution Hi-C Experiments. Cell Syst. *3*, 95–98.

48. Robinson, J.T., Turner, D., Durand, N.C., Thorvaldsdóttir, H., Mesirov, J.P., and Aiden, E.L. (2018). Juicebox.js Provides a Cloud-Based Visualization System for Hi-C Data. Cell Syst. *6*, 256–258.e1.

49. Abdennur, N., and Mirny, L.A. (2020). Cooler: scalable storage for Hi-C data and other genomically labeled arrays. Bioinformatics *36*, 311–316.

50. Open, 2C, Abdennur, N., Abraham, S., Fudenberg, G., Flyamer, I.M., Galitsyna, A.A., Goloborodko, A., Imakaev, M., Oksuz, B.A., and Venev, S.V. (2022). Cooltools: enabling high-resolution Hi-C analysis in Python. Preprint at bioRxiv.

51. Flyamer, I.M., Illingworth, R.S., and Bickmore, W.A. (2020). Coolpup.py: versatile pile-up analysis of Hi-C data. Bioinformatics *36*, 2980–2985.

52. Pradhan, B., Barth, R., Kim, E., Davidson, I.F., Bauer, B., van Laar, T., Yang, W., Ryu, J.K., van der Torre, J., Peters, J.M., et al. (2022). SMC complexes can traverse physical roadblocks bigger than their ring size. Cell Rep. *41*, 111491.

53. Virtanen, P., Gommers, R., Oliphant, T.E., Haberland, M., Reddy, T., Cournapeau, D., Burovski, E., Peterson, P., Weckesser, W., Bright, J., et al. (2020). SciPy 1.0: fundamental algorithms for scientific computing in Python. Nat. Methods *17*, 261–272.

54. Nakato, R., and Sakata, T. (2021). Methods for ChIP-seq analysis: A practical workflow and advanced applications. Methods *187*, 44–53.

55. Langmead, B., Trapnell, C., Pop, M., and Salzberg, S.L. (2009). Ultrafast and memory-efficient alignment of short DNA sequences to the human genome. Genome Biol. *10*, R25.

56. Siow, C.C., Nieduszynska, S.R., Müller, C.A., and Nieduszynski, C.A. (2012). OriDB, the DNA replication origin database updated and extended. Nucleic Acids Res. *40*, D682–D686.

57. McGuffee, S.R., Smith, D.J., and Whitehouse, I. (2013). Quantitative, genome-wide analysis of eukaryotic replication initiation and termination. Mol. Cell *50*, 123–135.

58. Clausen, A.R., Lujan, S.A., Burkholder, A.B., Orebaugh, C.D., Williams, J.S., Clausen, M.F., Malc, E.P., Mieczkowski, P.A., Fargo, D.C., Smith, D.J., et al. (2015). Tracking replication enzymology in vivo by genome-wide mapping of ribonucleotide incorporation. Nat. Struct. Mol. Biol. *22*, 185–191.

STAR★METHODS

KEY RESOURCES TABLE

REAGENT or RESOURCE	SOURCE	IDENTIFIER
Antibodies		
Mouse monoclonal anti-HA, clone 12CA5	Roche	Cat#1666606; RRID: AB_514505
Mouse monoclonal anti-c-Myc	Merck	Cat#M4439; RRID: AB_439694
Mouse monoclonal anti-FLAG M2	Merck	Cat#F1804; RRID: AB_262044
Chemicals, peptides, and recombinant proteins		
α-factor mating pheromone (custom peptide WHWLQLKPGQPMY)	Merck	N/A
Methyl 1-(butylcarbamoyl)-2-benzimidazolecarbamate (benomyl)	Merck	Cat#381586
3-indoleacetic acid (auxin)	Merck	Cat#I2886
Doxycycline hyclate	Merck	Cat#D9891
Thiolutin	Abcam	Cat#ab143556
Trichloroacetic acid	Merck	Cat#T6399
Formaldehyde	Merck	Cat#F8775
Dynabeads Protein A	Invitrogen	Cat#10002D
IgG Sepharose 6 FF	VWR	Cat#17-0969-01
Calmodulin Sepharose 4B	Merck	Cat#GE17-0529-01
Vivaspin 20 100K MWCO ultrafiltration unit	Sartorius	Cat#VS2041
Octameric Smc5/6	This study	N/A
Hexameric Smc5/6	This study	N/A
SNAP-Surface-Alexa Flour 647	New England Biolabs	Cat#S9136S
3-[(2-aminoethyl)aminopropyl] trimethoxysilane	Merck	Cat#8191720100
MethoxyPEG-N-hydroxysuccinimide	Laysan Bio, Inc	Cat#166-162
Biotin-PEG-N-hydroxysuccinimide	Laysan Bio, Inc	Cat#170-07
Streptavidin	Thermo Fisher Scientific	Cat#434301
Sytox Orange	Thermo Fisher Scientific	Cat#S34861
DpnII	New England Biolabs	Cat#R0543M
Critical commercial assays		
NEBNext Ultra II DNA Library Prep Kit for Illumina	New England Biolabs	Cat#E7645
Fast SYBR™ Green Master Mix	Applied Biosystems	Cat#4385612
Deposited data		
ChIP-seq data	This study	NCBI's Gene Expression Omnibus: GSE235560
RNA-seq	This study	NCBI's Gene Expression Omnibus: GSE235560
Hi-C data	This study	NCBI's Gene Expression Omnibus: GSE235560
Imaging data from single-molecule and western blot analyses	This study	Mendeley data: https://doi.org/10.17632/xm79hh8p65.1
Experimental models: Organisms/strains		
S. cerevisiae strains, see Table S1	This study	N/A
Oligonucleotides		
ChIP-qPCR and RT-PCR primers, see Table S2	This study	N/A
Recombinant DNA		
42 kb of coilable DNA	Kim et al.[34]	N/A

(*Continued on next page*)

Continued

REAGENT or RESOURCE	SOURCE	IDENTIFIER
Software and algorithms		
Bowtie2 version 2.4.1	Langmead and Salzberg[45]	N/A
RandomForest package	Liaw and Wiener[46]	N/A
Juicer	Durand et al. [47]	N/A
Juicebox	Robinson et al.[48]	N/A
hic2cool version 0.8.3	Abdennur and Mirny[49]	N/A
Balance algorithm in cooler version 0.8.11	Abdennur and Mirny[49]	N/A
Expected-cis algorithm in cooltools version 0.5.4	Open, 2C et al.[50]	N/A
plotpup.py in coolpup.py version 1.0.0.	Flyamer et al.[51]	N/A
Arrowhead algorithm in Juicer	Durand et al.[47]	N/A
Python based custom software	Pradhan et al.[52]	N/A
"find_peaks" algorithm in Scipy	Virtanen et al.[53]	N/A

RESOURCE AVAILABILITY

Lead contact

Further information and requests for resources and reagents should be directed to and will be fulfilled by the lead contact, Kristian Jeppsson (jeppsson@iqb.u-tokyo.ac.jp).

Materials availability

Yeast strains generated for this study are available upon request to the lead contact.

Data and code availability

- ChIP-seq, RNA-seq and Hi-C data have been deposited in NCBI's Gene Expression Omnibus. The data is accessible through the accession number Gene Expression Omnibus: GSE235560 (https://www.ncbi.nlm.nih.gov/geo/query/acc.cgi?acc=GSE235560). Imaging data from single-molecule and western blot analyses have been deposited at Mendeley and the DOI is listed in the key resources table. All deposited data is publicly available as of the date of publication.
- This paper does not report original code.
- Any additional information required to reanalyze the data reported in this paper is available from the lead contact upon request.

EXPERIMENTAL MODEL AND STUDY PARTICIPANT DETAILS

The *in vivo* experiments were performed in budding yeast *S. cerevisiae* of W303 origin (*ade2-1 trp1-1 can1-100 leu2-3,112 his3-11,15 ura3-1 RAD5*) with the modifications listed in Table S1. Purified hexameric and octameric *S. cerevisiae* Smc5/6 complexes were used in the single molecule analysis.

METHOD DETAILS

Yeast growth conditions, protein degradation, and transcription inhibition

Cells were cultured in YEP medium (1 % yeast extract, 2 % peptone, 40 μg ml^{-1} adenine) supplemented with 2 % glucose, or 2 % galactose, as stated, and at 30°C if not stated otherwise. For synchronization in G1-phase, 3 μg ml^{-1} α-factor mating pheromone (Merck, custom peptide WHWLQLKPGQPMY) was added every hour (a total of three additions) to cells growing logarithmically. For G2/M cell cycle arrest, benomyl (Merck, 381586) was added to the YEPD media for a final concentration 80 μg ml^{-1}. A complete G2/M-arrest of logarithmically growing cells was achieved after 90 minutes at 30°C, or 120 minutes at 23°C. For G2/M-arrest following synchronization in G1-phase, cells were released into benomyl-containing YEPD for 60 minutes. For depletion of Scc2, Wpl1, Top1, Smc6, Nse4, Nse5 and Top2 in Figures 1A, 1D, 4A, S2J, and S6C, auxin (3-indoleacetic acid, 1 mM final concentration, Merck, I2886) and doxycycline (5 μg ml^{-1} final concentration, Merck, D9891) were added to simultaneously degrade the proteins and inhibit their transcription, respectively. For degradation of Smc5 and Smc6 in Figure S5B, auxin (3-indoleacetic acid, Merck, I2886) was added at a final concentration of 1 mM. For transcription inhibition, thiolutin (Abcam, ab143556) was added to cell cultures for the final concentration of 20 μg ml^{-1} for 30 minutes. Cell cycle progression and arrests were confirmed using standard protocol for FACS analysis of ethanol-fixed, propidium iodide-stained cells.

Protein extraction and western blot

Depletion of HA-tagged Scc2, Wpl1, Top1, Smc6, Nse4, Nse5 and Top2 or degradation of MYC-tagged Smc5 and Smc6 were monitored by western blot using anti-HA antibody clone 12CA5 (Roche, 1666606), or anti-c-Myc antibody (Merck, M4439), respectively, after protein extraction by trichloroacetic acid (TCA)-precipitation. The 0-hour auxin+doxycycline (or auxin only, as in Figure S5B) western blot control samples were harvested immediately prior to the addition of the chemicals. Uncropped western blot images are found in Figure S7.

Chromatin immunoprecipitation, qPCR, and ChIP-seq library preparation

Chromatin immunoprecipitation was performed as detailed in Jeppsson et al..[17] Briefly, *S. cerevisiae* cells were crosslinked with 1 % formaldehyde for 30 minutes at room temperature, followed by incubation at 4°C overnight. Chromatin was then sheared to a size of 300-500 bp by sonication (Bandelin Sonopuls HD 2070.2) and IP reactions containing anti-FLAG antibody (Merck, F1804) conjugated to Dynabeads Protein A (Invitrogen, 10002D), were allowed to proceed overnight at 4°C. After completing the immunoprecipitation and reversing crosslinks, the DNA was purified. ChIP-qPCR was performed using Fast SYBR Green (Applied Biosystems, 4385612) and primers listed in Table S2, using an Applied Biosystem 7500 Real-Time PCR System according to the manufacturer's instructions. For ChIP-seq, DNA from ChIP and input fractions were prepared for sequencing using the NEBNext Ultra II DNA Library Prep Kit for Illumina (NEB, E7645). The libraries were sequenced using the HiSeq 2500 platform to generate single-end 65 bp reads. Sequenced reads were mapped to the *S. cerevisiae* genome using Bowtie2 version 2.4.1 with the default parameter set.[45] The numbers of total and mapped reads in each sample are listed in Table S3.

ChIP-seq data analysis

To call chromosome arm peaks for Smc6 in *top2-4*, and Scc1 in wild-type cells, we identified bins in which the fold enrichment (ChIP / input) was more than 2.0 in the dataset 2017_036B_1367-X, and 2017_034B_234-X, respectively. Peaks overlapping with long terminal repeats, and pericentromeric regions (25 kb spanning each centromere), were excluded. The Smc5/6 binding sites in *top2-4* cells were used for the average enrichment-, and *cis* interaction analyses in Figures 1F, 2F, 4C, 7G, S2E, and S6F. The cohesin binding sites in wild-type cells were used for the average peak plot-, pile-up plot- and domain number analyses in Figures 7F, 7J, 7M, S2I, and S6A. The 2691 ORFs used for the analysis of average Rpo21-FLAG enrichment in Figure 2B were selected to have average Rpo21 ChIP / input fold enrichment higher than 1.0 in wild-type cells, prior to the addition of thiolutin, *i.e.*, dataset 2017_035A_1958-2_0. We used DROMPAplus version 1.8. for normalizing, peak-calling, average enrichment analysis, and visualizing ChIP-seq data.[54]

RNA extraction, quantitative reverse-transcription PCR, and sequencing

Total RNA was prepared from $2.5x10^8$ yeast cells with Trizol (Invitrogen) and RNA extraction was performed according to the manufacture's description. Briefly, 1 ml of Trizol reagent was added to the cells and cell disruption was achieved through vortexing (2 minutes) in the presence of glass beads. Then, 0.2 ml of chloroform was added to the cell suspension and incubated for 2 minutes at room temperature. Samples were centrifuged at 12,000 g for 15 minutes at 4°C and the aqueous phase was transferred to a fresh tube and mixed with 0.5 ml isopropanol. For RNA precipitation, samples were incubated at room temperature for 10 minutes and centrifuged at 12,000 g for 10 minutes at 4°C. RNA pellets were then washed with 70 % ethanol, air-dried and dissolved in 50 μl RNase-free water. cDNA for quantitative reverse-transcription was prepared using the High-Capacity cDNA Reverse Transcription Kit (ABI) according to the manufacture's guidelines. qPCR for *MCR1*, *DBR1* and *ACT1* was performed using SYBR green (ABI) and primers listed in Table S2 on Applied Biosystem 7000 Real-Time PCR System, according to the manufacture's guidelines. RNA-seq samples were prepared according to the manufacture's standard protocol (TruSeq Standard Total RNA Sample Prep Kit, Illumina). Amplified cDNA was sequenced using the Illumina HiSeq platform (HiSeq2000) to generate single-end 50 bp reads. Sequence reads were aligned to the *S. cerevisiae* genome obtained from Saccharomyces Genome Database (http://www.yeastgenome.org/) using Bowtie,[55] with the default parameters. The numbers of total and mapped reads in each sample are listed in Table S3.

Quantitative modeling of ChIP-seq data

Mathematical models to recapitulate Scc1 and Smc6 ChIP-seq profiles were constructed by a machine-learning algorithm. Since most of the Scc1 and Smc6 ChIP-seq peaks were located in the intergenic regions (IGRs),[14] we focused on the Scc1 and Smc6 binding to IGRs. ChIP-seq fold-enrichment (FE) was calculated for each 10-bp bin in the genome, and the maximum FE within a 1 kb window centred on the midpoint of each IGR was used as the target variable. For predictor variables, 47 features associated with each IGR were calculated and used (summarized in Table S4). The data used for the feature calculation includes replication origin location in oriDB,[56] replication fork merging zone,[57] replication fork polarity,[58] as well as RNA-seq data from wild-type and *top2-4* cells arrested in G2/M after an S-phase at 35°C, restrictive temperature for the *top2-4* allele, obtained in this study. We built random forest regression models based on all or some of the features. The randomForest package in the R programming language was used for computing.[46] The hyperparameter mtry was tuned by the tuneRF function. Model construction and evaluation were conducted by stratified fourfold cross-validation and iterated five times with differently split datasets. Spearman's rank correlation coefficient (ρ) between the predicted and observed FE values was used for the evaluation of modelling accuracy.

Smc5/6 complex purification and labelling

Hexameric (Smc5, Smc6, Nse1, Nse2, Nse3 and Nse4) and octameric (Smc5, Smc6, Nse1, Nse2, Nse3, Nse4, Nse5 and Nse6) *S. cerevisiae* Smc5/6 complexes were purified using the yeast overexpression protocol detailed in Pradhan et al..[3] Similarly, the fluorescently labelled Smc5/6 complexes which carry a C-terminal SNAP-tag on the Nse4 subunit were overexpressed, purified, and labelled as detailed in Pradhan et al..[3] Briefly, the Smc5/6 subunits under the control of Gal1-10 promoter were overexpressed in *S. cerevisiae* by adding 2 % galactose to exponentially growing yeast cells in YEP-lactate medium, and subsequently isolated by tandem affinity purification using IgG Sepharose 6 FF (VWR, 17-0969-01) and calmodulin Sepharose 4B (Merck, GE17-0529-01). The eluate was concentrated using Vivaspin 20 100K MWCO ultrafiltration unit (Sartorius, VS2041), with simultaneous exchange to the buffer used for storage. For fluorescent labeling of the complexes, the eluate obtained from IgG Sepharose 6 FF was incubated with SNAP-Surface-Alexa Flour 647 (New England Biolabs, S9136S) at 4°C overnight. The resulting mixture was further purified and concentrated using Vivaspin 20 100K MWCO ultrafiltration unit concomitant with buffer exchange.

Single-molecule loop extrusion assay

The single-molecule experiment with supercoiled DNA was performed by building on methods described in Pradhan et al.[3] and Kim et al..[34] In essence, the process is split into three stages: surface functionalization, flow cell creation, and the loop extrusion assay with DNA supercoils. We used a custom-made HiLO (highly inclined optical light sheet) microscope for imaging, as per Pradhan et al..[3] During surface functionalization, we first prepared glass coverslips through silanization using a solution of 1% 3-[(2-aminoethyl)aminopropyl] trimethoxysilane in methanol and 5% glacial acetic acid. This was done after cleaning the coverslips with potassium hydroxide and acid piranha. Afterwards, we treated the silanized coverslips with a solution of 100mg/mL methoxy-PEG-N-hydroxysuccinimide and 1 mg/mL biotin-PEG-N-hydroxysuccinimide in ice-cold borate buffer at pH 8.5. After overnight incubation, we rinsed the coverslips with milliQ water and dried them using nitrogen gas. This PEGylation was repeated five times before we sealed and stored the slides at -20 °C until use. For flow cell assembly, we drilled holes into slides to accommodate pipette tips. The same cleaning and functionalization processes were applied to these slides as to the coverslips. Flow channels were constructed using double-sided tape to sandwich the coverslip and slide together. One end of the resulting channel was connected to a syringe pump via a tube, and any openings, barring the drilled holes, were sealed to prevent sample leakage.

For the loop extrusion assay, we used 42 kb of coilable DNA (without nicks), with biotin ligated to both ends. We anchored the DNA to the coverslip by incubating 1 μM streptavidin in T50 buffer (40 mM Tris pH 7.5, 50 mM NaCl, 0.1 mM EDTA) within the channel, followed by a thorough wash. We then introduced a buffer at 3 μL/min containing the biotinylated DNA into the channel until we had a dense (but isolated, 100 DNA per 0.01 mm^2) double-tethered DNA fill on the surface. We used Sytox Orange (SxO) for visualization and inducing twists in the DNA, introducing different supercoiling based on the presence of SxO in the imaging buffer. To find a SxO concentration inducing equivalent left-handed and right-handed twists, we plotted a titration curve (Figure S4A) using images of tethered DNA recorded at varying SxO concentrations using a 561 nm laser. We determined C1/2 ∼ 300 nM as the concentration where half of the intercalating sites are occupied, corresponding to half the maximum intensity. For negative supercoiling, DNA flowed at 800 nM SxO at 1.5 μL/min in the imaging buffer, occupying most intercalating sites. We maintained a final concentration of 300 nM SxO for both positive and negative supercoils during the loop extrusion assay.

Videos consisting of 10,000 frames at an acquisition speed of 100 ms per frame were recorded in the presence of 0.5 nM Smc5/6 hexamer or octamer combined with 2 mM ATP in the imaging buffer. Similarly, 2 nM hexamer tagged with Alexa647 and 2 mM ATP in the imaging buffer was introduced while alternating excitation between 561 nm and 640 nm lasers. For side-flow visualization, we employed a three ways channel, applying a flow of 20 μL/min perpendicular to the axis of the anchored DNA.

Hi-C library preparation

Hi-C was performed as detailed in Jeppsson et al..[17] Briefly, *S. cerevisiae* cells were crosslinked with 3 % formaldehyde for 20 minutes at room temperature. Following spheroplasting and gentle lysis, restriction digestion of crosslinked chromatin by DpnII (NEB, R0543M) was performed overnight at 37°C, after which the restriction enzyme was inactivated by incubation at 62°C for 20 minutes. The presence of intact and individual DNA masses throughout the spheroplasting, digestion, and ligation steps were confirmed by DAPI (4′,6-diamidino-2-phenylindole)-staining and microscopy. Marking and repairing DNA ends, proximity ligation, crosslink reversal, DNA shearing, size selection, biotin pull-down, preparation for Illumina sequencing, final amplification (15 cycles) and purification were then performed as in Jeppsson et al.[17] The Hi-C libraries were sequenced on Illumina HiSeq series with 150-bp paired-end sequencing according to the manufacturer's recommendations. The numbers of total and mapped read pairs for each sample are listed in Table S5.

Hi-C data analysis

The Hi-C data were processed using Juicer with the default parameter set.[47] The sequenced reads were mapped to the *S. cerevisiae* genome obtained from Saccharomyces Genome Database (SGD) (http://yeastgenome.org/). The uniquely mapped read pairs were randomly resampled and arranged in the same numbers within sample groups (see Table S5). Contact matrices used for further analysis were coverage (sqrt)–normalized at 1- and 2-kb resolution with Juicer. The matrices were visualized by Juicebox.[48] Intrachromosomal contact frequency distribution was calculated using nonduplicated valid Hi-C contact pairs at genomic distances increasing by 1 kb.

Pile-up plots of pixels corresponding to pairs of specific sites in the contact matrices were calculated and normalized to the expected signal of global *cis* interactions at 1-kb resolution. Briefly, .cool format files were obtained from .hic format files by using hic2cool version 0.8.3 and the obtained matrices were normalized using the balance algorithm in cooler version 0.8.11.[49] Expected Hi-C signals for *cis* interactions were calculated from these matrices using the expected-cis algorithm in cooltools version 0.5.4.[50] Pile-up plots were then calculated using coolpup.py with "–flank 15000 –mindist 0" option and plotted using plotpup.py in coolpup.py version 1.0.0.[51]

Domains were identified by using the Arrowhead algorithm in Juicer with coverage (sqrt) normalization at 1- and 2-kb resolution with "-m 300 -k VC_SQRT -r 2000" and "-m 200 -k VC_SQRT -r 1000" option. The Arrowhead detects the corners of the domains to identify their boundaries. The candidate domains at 1- and 2-kb resolution were merged, and the domains overlapping with Scc1 binding sites at both up- and downstream boundaries were used in the subsequent analysis.

The number of uniquely mapped *cis* and *trans* read pairs was normalized by total read number (read pair per kilobase). For *cis* interactions at Smc5/6 binding sites, uniquely mapped *cis* read pairs overlapping with these regions at either or both up- and downstream sites were obtained, and the number was normalized by total read number (read pair per million mapped read pairs).

QUANTIFICATION AND STATISTICAL ANALYSIS

ChIP-qPCR and Hi-C data

For ChIP-qPCR, two-sided t-test was used for analysis, and mean values from biological triplicates with error bars representing standard deviation are shown in the presented graphs. Binomial tests were used for the analysis of chromosomal *cis* / *trans* interactions, detected by Hi-C.

Single-molecule loop extrusion assay

Microscopy images containing 10s of tethered DNAs in a field of view were examined to identify nicked and plectonemic DNA. DNAs exhibiting uniform intensity along their axis were categorized as nicked, whereas those with dynamic puncta were deemed plectonemic. Regions containing nicked and plectonemic DNA were isolated and saved as TIFF file for further quantification, using the Python based custom software described in Pradhan et al..[52] Specifically, we created kymographs by accumulating intensities on 11 pixels across the DNA axis and stacking each line of intensity for each image frame (see Figure 6B for an example). We located peak intensities corresponding to each punctum along the DNA axis using the "find_peaks" algorithm in Scipy.[53] We calculated the area under each peak by summing intensities on 9 pixels around the peak to derive the puncta intensity (I_{puncta}), while summing the remaining pixels gave the intensities outside the puncta (I_{out}). We estimated puncta size as I_{puncta} (kb) = 42kb * $I_{puncta}/(I_{puncta}+I_{out})$. We identified any punctum that localized to a single spot and increased in size upon Smc5/6 addition as a loop, determining its size using a similar method: I_{loop}(kb) = 42kb * $I_{loop}/(I_{loop}+I_{out})$. The loop size over time (t) provided the loop extrusion kinetics, and fitting the initial linear slope with the formula $I_{loop} = k*t$ yielded the loop extrusion rate (k).

For labeled Smc5/6, we obtained kymographs for both the 561 nm (DNA) and 640 nm excitations. We extracted the intensities at the same positions as the DNA puncta or loops from the 640 nm excited kymograph, yielding time traces (see Figures 6F and 6G for an example) that facilitated estimating the number of hexamers involved in loop extrusion.